Spectral and transport properties of doped Mott-Hubbard systems with incommensurate magnetic order

Fleck, Marcus; Lichtenstein, Alexander I.; Olés, Andrzej M.; Hedin, Lars

Published in:
Physical Review B

DOI:
10.1103/PhysRevB.60.5224

1999

Spectral and transport properties of doped Mott-Hubbard systems with incommensurate magnetic order

Marcus Fleck and Alexander I. Lichtenstein
Max-Planck-Institut für Festkörperforschung, Heisenbergstrasse 1, D-70569 Stuttgart, Federal Republic of Germany

Andrzej M. Oleś
Institute of Physics, Jagellonian University, Reymonta 4, PL-30059 Kraków, Poland
and Max-Planck-Institut für Festkörperforschung, Heisenbergstrasse 1, D-70569 Stuttgart, Federal Republic of Germany

Lars Hedin
Department of Theoretical Physics, University of Lund, Solvegatan 14A, S-22362 Lund, Sweden
and Max-Planck-Institut für Festkörperforschung, Heisenbergstrasse 1, D-70569 Stuttgart, Federal Republic of Germany
(Received 11 November 1998; revised manuscript received 26 April 1999)

We present spectral and optical properties of the Hubbard model on a two-dimensional square lattice using a generalization of dynamical mean-field theory to magnetic states in a finite dimension. The self-energy includes the effect of spin fluctuations and screening of the Coulomb interaction due to particle-particle scattering. At half-filling the quasiparticles reduce the width of the Mott-Hubbard ''gap'' and have dispersions and spectral weights that agree remarkably well with quantum Monte Carlo and exact diagonalization calculations. Away from half-filling we consider incommensurate magnetic order with a varying local spin direction, and derive the photoemission and optical spectra. The incommensurate magnetic order leads to a pseudogap which opens at the Fermi energy and coexists with a large Mott-Hubbard gap. The quasiparticle states survive in the doped systems, but their dispersion is modified by the doping, and a rigid-band picture does not apply. Spectral weight in the optical conductivity is transferred to lower energies, and the Drude weight increases linearly with increasing doping. We show that incommensurate magnetic order also leads to midgap states in the optical spectra and to decreased scattering rates in the transport processes, in qualitative agreement with the experimental observations in doped systems. The gradual disappearence of the spiral magnetic order and the vanishing pseudogap with increasing temperature is found to be responsible for the linear resistivity. We discuss the possible reasons why these results may only partially explain the features observed in the optical spectra of high-temperature superconductors. [S0163-1829(99)04632-9]

I. INTRODUCTION

In the past decade interest in the physical properties of correlated electronic systems has greatly increased. One reason for this is the strong local correlations on transition-metal ions in cuprate superconductors and manganites, and the corresponding unusual properties of these compounds. The parent undoped compounds are Mott-Hubbard or charge-transfer insulators, while doping leads to correlated metals in which the kinetic energy of charge carriers competes with magnetic order.[1] One of the most spectacular consequences is the onset of high-temperature superconductivity in the cuprates. It is believed that a satisfactory description of the normal phase properties is a prerequisite for the understanding of the microscopic mechanism of pairing in high-temperature superconductors. The electronic states in CuO_2 planes of cuprate superconductors are usually described in terms of the Emery model, which includes hybridization between Cu($3d_{x^2-y^2}$) and O($2p_{x(y)}$) states.[2] However, hole doping leads to the formation of local Zhang-Rice singlets,[3] and the essential excitations in the cuprates within a window of a few eV around the chemical potential are well reproduced using an effective two-dimensional (2D) Hubbard model with extended hopping[4] and a large local Coulomb interaction U, as shown by various numerical studies of the t-J and Hubbard models.[5]

Recently it was shown[4,6,7] that the effective Hubbard model has to include hopping beyond nearest neighbors. The second-nearest-neighbor hopping changes the dispersion of the quasiparticle (QP) states, and is therefore crucial for understanding angular-resolved photoemission (ARPES) data of the antiferromagnetic (AF) insulator $Sr_2CuO_2Cl_2$.[6] Both second- and third-neighbor hopping parameters follow from the down-folding procedure in electronic structure calculations,[7] and influence the shape of the Fermi surface. They have a particular relation to the value of the superconducting transition temperature at optimal doping.[8]

The superconductivity occurs in the cuprates under doping $\delta=1-n$ of a half-filled ($n=1$) AF insulator, and is accompanied by a gradual modification of the magnetic order. The nature of magnetic correlations in doped materials is therefore a central issue in the theory of the cuprate superconductors. Undoped La_2CuO_4 is a *commensurate* AF insulator, while doping by Sr into $La_{2-x}Sr_xCuO_4$ results in short-range AF order within *incommensurate* magnetic structures.[9,10] Such an incommensurate magnetic order was indeed found analytically,[11,12] in Hartree-Fock (HF)[13,14] and slave-boson approximations.[14–17] However, in order to understand the transport properties, one has to go beyond an effective single-particle description and include the dynamics due to local electron correlations.

A sufficiently accurate treatment of local electron correlations remains one of the challenging problems in modern solid-state theory. Although important progress in the present understanding of strongly correlated fermion systems occurred recently due to numerical methods, such as quantum Monte Carlo (QMC) and exact diagonalization (ED), an analytic treatment that maintains local correlations is needed to investigate the consequences of strong correlations in the thermodynamic limit. An attractive possibility is the limit of large spatial dimension ($d=\infty$), where the diagrams in the perturbative expansion collapse to a single site, and the fermion dynamics is described by a *local self-energy*.[18] This allows a mapping of lattice models onto quantum impurity models, which can then be solved self-consistently using dynamical mean-field theory (DMFT).[19]

DMFT was quite successful for the Hubbard model with nearest-neighbor hopping t at half-filling, where it predicts the Mott transition to the insulating state ($n=1$).[20] This was also found by Logan, Eastwood, and Tusch[21] for the $d=\infty$ case using an analytic method. Attempts to use DMFT at arbitrary filling, however, made it clear that the local self-energy becomes particularly important in systems with magnetic long-range order (LRO), which are easily destabilized when the correlation effects are overestimated. The self-energy therefore plays a decisive role, and has to be described *beyond* second-order perturbation theory (SOPT).[22,23] This has made the application of DMFT to magnetically ordered systems notoriously difficult. Recently we have shown that the screening of local Coulomb interaction by the particle-particle diagrams plays a crucial role in stabilizing the incommensurate magnetic LRO in doped systems.[24]

The advantage of using DMFT becomes clear by looking at the single-hole problem, which can be solved exactly in the $d\rightarrow\infty$ limit.[25] The method becomes exact because the quantum fluctuations are of higher order in the $1/d$ expansion than the leading potential term which originates from the Ising part of the superexchange interaction $J=4t^2/U$. Therefore, applying DMFT to the $d=2$ case might still capture the essential features that result from the coupling of a moving hole to local spin fluctuations. We will show below that in fact such quantities as the spectral function, the QP band, and the size of the QP spectral weight are well reproduced within DMFT, which for a single hole includes only those processes which are present in the t-J_z model. Although this approach becomes exact only in the $d\rightarrow\infty$ limit,[25] it gives a sufficient accuracy of the one-particle spectral function even in a finite dimension $d=2$.[26] DMFT allows us to calculate the optical conductivity in the $d=\infty$ limit of Metzner and Vollhardt[18] from the knowledge of the local self-energy without further approximations.[27] The studies performed in this limit for nonmagnetic systems already allowed a qualitative reproduction of such experimental observations in the cuprates as the increase of the Drude peak with doping, and a temperature- and doping-dependent midinfrared peak.[28,29]

This paper is organized as follows. The self-consistent procedure to determine a local self-energy within DMFT is introduced in Sec. II. It consists of the HF potential and the dynamical part due to spin fluctuations which uses a Coulomb interaction renormalized by particle-particle scattering. The formalism to calculate the one-particle and optical excitation spectra in the spin spiral states is developed in Sec. III. Next we analyze the numerical results for the one-particle spectral properties in Sec. IV, where we show how they change with doping and with increasing temperature. The optical properties are presented in Sec. V; there we discuss effects in the optical conductivity, scattering rate, and effective mass which arise due to extended hopping and by increasing the value of Coulomb interaction U. Section VI presents a short summary and conclusions.

II. DYNAMICAL MEAN-FIELD THEORY FOR SPIN SPIRAL ORDER

A. Dynamical mean-field equations

We consider the spectral and optical properties of the minimal model for strongly correlated electrons in high-temperature superconductors, the Hubbard model with extended hopping,[4,7]

$$H=-\sum_{ij\sigma} t_{ij}a^{\dagger}_{i\sigma}a_{j\sigma}+U\sum_{i} n_{i\uparrow}n_{i\downarrow}, \tag{2.1}$$

where $a^{\dagger}_{i\sigma}$ is a creation operator of an electron with spin σ at site i, and $n_{i\sigma}=a^{\dagger}_{i\sigma}a_{i\sigma}$. The hopping elements $t_{ij}=t$, t' and t'' stand for the nearest-neighbor, second-nearest-neighbor, and third-nearest-neighbor hopping on a 2D square lattice, and serve to model the electronic states of the charge-transfer type in the cuprates. For convenience we choose t as the energy unit.

It is interesting to note that hopping beyond nearest neighbors contributes to the energy and other properties not only in a 2D model, but also in the limit of $d\rightarrow\infty$. The energy contributions due to more distant neighbors are finite due to the scaling of the hopping parameters on a hypercubic lattice. It is given by $t_{ij}\sim d^{-\|i-j\|/2}$ (see Refs. 18 and 30), where $\|i-j\|$ is the distance between i and j defined by the ''bond metric,'' and gives the scaling factors $\sim 1/\sqrt{d}$ for first-neighbor hopping and $\sim 1/d$ for second- and third-nearest neighbor hopping, as the latter sites are two bonds apart.

As mentioned above, we adopt the limit of infinite dimensions to determine the spectral properties of the Hubbard Hamiltonian on a square lattice in the thermodynamic limit. In order to simplify the numerical evaluation of the self-energy, we introduce an ansatz for the modified magnetic order in the doped systems, and assume incommensurate SS structures with a large but finite periodicity. This approach captures the essence of the competition between the weakened short-range AF order, and the kinetic energy induced by hole doping,[14] and allows us to treat the systems in the thermodynamic limit at low temperature. The spiral states are characterized by the amplitude of the local magnetization,

$$m_0=|\langle n_{i\uparrow}-n_{i\downarrow}\rangle|, \tag{2.2}$$

which is independent of the site index i. The direction of the magnetic moment at each site i is specified in the *global reference frame* by two spherical angles, $\Omega_i=(\phi_i,\theta_i)$, and, therefore, the original fermion operators, $\{a^{\dagger}_{i\uparrow},a^{\dagger}_{i\downarrow}\}$, are transformed to fermions quantized with respect to *the local quantization axis* at each site,[14]

$$c^{\dagger}_{i\sigma}=\sum_{\lambda}\; a^{\dagger}_{i\lambda}[\mathcal{R}(\Omega_i)]_{\lambda\sigma}, \tag{2.3}$$

where $\mathcal{R}(\Omega_i)=e^{-i(\phi_i/2)\hat{\sigma}_z}e^{-i(\theta_i/2)\hat{\sigma}_y}$ is the rotation matrix, ϕ_i and θ_i are polar and azimuthal angle, respectively, and $\hat{\sigma}_y$ and $\hat{\sigma}_z$ are Pauli spin matrices. This transforms the Hubbard Hamiltonian (2.1) to the following form:

$$H=-\sum_{ij,\sigma\sigma'}\; t_{ij}c^{\dagger}_{i\sigma}[\mathcal{R}^{\dagger}(\Omega_i)\mathcal{R}(\Omega_j)]_{\sigma\sigma'}c_{j\sigma'}+U\sum_{i}\; n_{i\uparrow}n_{i\downarrow}\,. \tag{2.4}$$

In the SS states we take the polar angle to be site independent, $\theta_i=\theta$, and the azimuthal angle is given by the wave vector $\mathbf{Q}$ of the spiral; $\phi_i=\mathbf{Q}\cdot\mathbf{R}_i$. Using the periodicity of the $\mathcal{R}^{\dagger}\mathcal{R}$ matrix in Eq. (2.4), after a Fourier transformation one finds that the kinetic energy takes a simple 2×2 matrix form,

$$\hat{T}_{\mathbf{Q}}(\mathbf{k})=\tfrac{1}{2}\varepsilon_{\mathbf{k}-(\mathbf{Q}/2)}(\hat{1}+\cos\theta\,\hat{\sigma}_z-\sin\theta\,\hat{\sigma}_x)+\tfrac{1}{2}\varepsilon_{\mathbf{k}+(\mathbf{Q}/2)}(\hat{1}-\cos\theta\,\hat{\sigma}_z+\sin\theta\,\hat{\sigma}_x), \tag{2.5}$$

where $\varepsilon_{\mathbf{k}}=-2t(\cos k_x+\cos k_y)-4t'\cos k_x\cos k_y-2t''(\cos 2k_x+\cos 2k_y)$ is the electron dispersion in a noninteracting system in the global reference frame. Here we limit ourselves to plane spirals, and choose $\theta=\pi/2$. Therefore, the order parameter rotates in the (a,b) plane, $\langle\mathbf{S}_i\rangle=(m_0/2)[\cos(\mathbf{QR}_i),\sin(\mathbf{QR}_i),0]$. Double spirals were shown to be unstable in the 2D t-J model,[15] and we have no reason to believe that they might be stabilized by further neighbor hopping.

In order to construct the leading local part of the self-energy, we use DMFT and consider the impurity model coupled to the lattice by the effective field (for more details, see Ref. 19). The Anderson model of a magnetic impurity coupled to a conduction band with SS order consists of a ''nondegenerate impurity orbital'' at site o, with the fermion operators $\{f^{\dagger}_{o\sigma},f_{o\sigma}\}$, and the conduction electron bath as an ''effective SS conduction band'' described by the operators $\{c^{\dagger}_{\mathbf{k}\sigma},c_{\mathbf{k}\sigma'}\}$

$$H_{imp}=\varepsilon_f\sum_{\sigma}\; f^{\dagger}_{o\sigma}f_{o\sigma}+\sum_{\mathbf{k}\sigma\sigma'}\; c^{\dagger}_{\mathbf{k}\sigma}[\tilde{T}_{\mathbf{Q}}(\mathbf{k})]_{\sigma\sigma'}c_{\mathbf{k}\sigma'}+\sum_{\mathbf{k}\sigma\sigma'}\;[f^{\dagger}_{o\sigma}[V_{\mathbf{Q}}(\mathbf{k})]_{\sigma\sigma'}c_{\mathbf{k}\sigma'}+\mathrm{H.c.}]+Un^{f}_{o\uparrow}n^{f}_{o\downarrow}\,, \tag{2.6}$$

where ε_f is an impurity energy level, and $\tilde{T}_{\mathbf{Q}}(\mathbf{k})$ is an effective one-particle energy of the same functional form as $\hat{T}_{\mathbf{Q}}(\mathbf{k})$ (2.5). The hybridization 2×2 matrix in the local reference frame,

$$\hat{V}_{\mathbf{Q}}(\mathbf{k})=\frac{1}{2}v_{\mathbf{k}-(\mathbf{Q}/2)}\left[\cos\frac{\theta}{2}(\hat{1}+\hat{\sigma}_z)-\sin\frac{\theta}{2}\hat{\sigma}_+\right]+\frac{1}{2}v_{\mathbf{k}+(\mathbf{Q}/2)}\left[\cos\frac{\theta}{2}(\hat{1}-\hat{\sigma}_z)+\sin\frac{\theta}{2}\hat{\sigma}_-\right], \tag{2.7}$$

where $\hat{\sigma}_{\pm}=\hat{\sigma}_x\pm i\hat{\sigma}_y$, is given by the individual hybridization elements in the global reference frame, $v_{\mathbf{k}}=\sum_i e^{i\mathbf{k}\cdot\mathbf{R}_i}v_{oi}$. Hamiltonian (2.6) is quadratic in $c_{\mathbf{k}\sigma}$, and the bath of conduction electrons can be integrated out giving rise to an effective action of the impurity electrons which is of the usual form[19]

$$S_{eff}=-\sum_{\sigma\sigma'}\;\int_0^{\beta}d\tau d\tau'\,\psi^{\star}_{o\sigma}(\tau)\mathcal{G}^{0}_{\mathbf{Q}\sigma\sigma'}(\tau-\tau')^{-1}\psi_{o\sigma'}(\tau')+U\int_0^{\beta}d\tau\; n^{f}_{o\uparrow}(\tau)n^{f}_{o\downarrow}(\tau), \tag{2.8}$$

where $\{\psi_{o\sigma},\psi^{\star}_{o\sigma'}\}$ are Grassmann variables for the f electrons. The *Weiss effective field* $\mathcal{G}^{0}_{\mathbf{Q}\sigma\sigma'}(\tau-\tau')$ is a 2×2 matrix in spin space,

$$\hat{\mathcal{G}}^{0}_{\mathbf{Q}}(i\omega_\nu)^{-1}=i\omega_\nu-\varepsilon_f-\sum_{\mathbf{k}}\;\hat{V}_{\mathbf{Q}}(\mathbf{k})[i\omega_\nu-\tilde{T}_{\mathbf{Q}}(\mathbf{k})]^{-1}\hat{V}^{\dagger}_{\mathbf{Q}}(\mathbf{k}). \tag{2.9}$$

For a plane spin spiral with $\theta=\pi/2$, the Weiss effective field becomes a diagonal matrix in spin space:

$$\mathcal{G}^{0}_{\mathbf{Q}\sigma\sigma'}(i\omega_n)\sim\delta_{\sigma\sigma'}\,. \tag{2.10}$$

Note that this result only depends on the functional form of Eqs. (2.5)–(2.7), and not on the parameters, except that it holds for a plane spiral. This implies that the local spin fluctuations are decoupled from the local charge fluctuations, and simplifies the present self-consistent calculation for SS states within the DMFT approach, as all local quantities including the self-energy Σ, are diagonal.

In the spirit of the DMFT approach, we approximate the Green function using a *local self-energy*[18,19]

$$\hat{G}^{-1}_{\mathbf{Q}}(\mathbf{k},i\omega_\nu)=i\omega_\nu+\mu-\hat{T}_{\mathbf{Q}}(\mathbf{k})-\hat{\Sigma}^{\mathrm{HF}}_{\mathbf{Q}}-\hat{\Sigma}^{\mathrm{SF}}_{\mathbf{Q}}(i\omega_\nu), \tag{2.11}$$

where $\mu=-\varepsilon_f$ is the chemical potential. The lattice (finite) dimensionality enters via the one-particle energies $\hat{T}_{\mathbf{Q}}(\mathbf{k})$, and gives rise to the $\mathbf{k}$ dependence of the spectral function. The lattice one-particle Green function (2.11) is described by a 2×2 matrix $\hat{G}_{\mathbf{Q}}(\mathbf{k},i\omega_\nu)$ in spin space, where ω_ν are fermionic Matsubara frequencies. The corresponding local lattice Green function, $\hat{G}_{\mathbf{Q}}(i\omega_\nu)=N^{-1}\Sigma_{\mathbf{k}}\hat{G}_{\mathbf{Q}}(\mathbf{k},i\omega_\nu)\propto\delta_{\sigma\sigma'}$, is diagonal in spin space due to the parity of the kinetic energy $\hat{T}_{\mathbf{Q}}(\mathbf{k})$.

The self-energy consists of the HF part $\Sigma^{\mathrm{HF}}_{\mathbf{Q}\sigma}=U\langle n_{0\bar{\sigma}}\rangle$, with $\bar{\sigma}=-\sigma$, and the spin-fluctuation (SF) part $\Sigma^{\mathrm{SF}}_{\mathbf{Q}\sigma}(i\omega_\nu)$, which is determined by the many-body effects. Using the *cavity method*[19] for a hypercubic lattice at $d=\infty$, we verified that the dynamical Weiss field $\mathcal{G}^{0}_{\mathbf{Q},\sigma}(i\omega_\nu)$ can be computed from the Dyson equation of the Anderson impurity model (2.6) with broken spin symmetry,

$$\hat{\mathcal{G}}^{0}_{\mathbf{Q}}(i\omega_\nu)^{-1}=\hat{G}_{\mathbf{Q}}(i\omega_\nu)^{-1}+\hat{\Sigma}^{\mathrm{SF}}_{\mathbf{Q}}(i\omega_\nu). \tag{2.12}$$

Equations (2.11) and (2.12) are fundamental in the DMFT,[19] and can be solved self-consistently, provided an expression for the self-energy is known.

B. Thermodynamic potential at finite temperature

The calculations at finite temperature T require the knowledge of the free energy, $F(T,N_e)$, being a thermodynamic potential for a system of $N_e=Nn$ electrons. It has to be minimized to find a stable SS state which determines the system properties. The free energy may be found from the grand canonical potential, $\Omega(T,\mu)$, using the standard approach for quantum many-body systems, $F(T,N_e)=\Omega(T,\mu)+\mu N_e$.[31] For a translationally invariant lattice model with *local self-energy* one finds the functional form of the grand canonical potential,

$$\Omega(T,\mu)=\Omega_0(T,\mu)+\Phi^{\mathrm{SF}}[\hat{G}_{\mathbf{Q}}]-\beta^{-1}\times\sum_{\mathbf{k}\nu}\ln\det[1-\hat{G}^0_{\mathbf{Q}}(\mathbf{k},i\omega_\nu)\hat{\Sigma}^{\mathrm{SF}}_{\mathbf{Q}}(i\omega_\nu)]-\beta^{-1}N\sum_{\nu}\mathrm{Tr}[\hat{\Sigma}^{\mathrm{SF}}_{\mathbf{Q}}(i\omega_\nu)\hat{G}_{\mathbf{Q}}(i\omega_\nu)], \quad (2.13)$$

with $\beta=1/k_BT$, and $\hat{\Sigma}^{\mathrm{SF}}_{\mathbf{Q}}(i\omega_\nu)$ is the self-energy discussed below. Functional (2.13) is stationary, i.e., $\delta\Omega=0$ ensures that the minimum of the grand canonical potential has been found, and determines the self-energy from the Luttinger-Ward functional,

$$\Sigma^{\mathrm{SF}}_{\sigma\sigma}[\hat{G}_{\mathbf{Q}}]=\frac{1}{N}\frac{\delta\Phi^{\mathrm{SF}}[\hat{G}_{\mathbf{Q}}]}{\delta\hat{G}_{\mathbf{Q},\sigma\sigma}}. \quad (2.14)$$

Our perturbative expansion is constructed around the symmetry-broken HF state, hence the grand canonical potential of the ''noninteracting'' reference system includes a correction term to avoid double counting, and reads

$$\Omega_0(T,\mu)=\beta^{-1}\sum_{\mathbf{k}\nu}\ln\det[\hat{G}^0_{\mathbf{Q}}(\mathbf{k},i\omega_\nu)]-UN\langle n_{o\uparrow}\rangle\langle n_{o\downarrow}\rangle. \quad (2.15)$$

The spectrum which defines $\Omega_0(T,\mu)$ is given by the Green's function in the HF approximation,

$$\hat{G}^0_{\mathbf{Q}}(\mathbf{k},i\omega_\nu)^{-1}=i\omega_\nu+\mu-\hat{T}_{\mathbf{Q}}(\mathbf{k})-\hat{\Sigma}^{\mathrm{HF}}_{\mathbf{Q}}. \quad (2.16)$$

The Luttinger-Ward functional $\Phi^{\mathrm{SF}}[G_{\mathbf{Q}}]$ in Eq. (2.13) is defined via the diagrammatic expansion of $\Sigma^{\mathrm{SF}}_{\mathbf{Q}}$ in terms of the full Green's function $G_{\mathbf{Q}}$. The self-energy of the infinite-dimensional Hubbard model is a local dynamical quantity, and involves only the local component of the Green's function (2.11). This implies that $\Phi^{\mathrm{SF}}[G]=N\Phi^{\mathrm{SF}}_{\mathrm{imp}}[G]$,[32] meaning that the functional $\Phi^{\mathrm{SF}}[G]$ can be approximated by some infinite subset of the one-particle irreducible closed Feynman diagrams of the Anderson impurity model (2.6). We take for $\Phi^{\mathrm{SF}}[G]$ we take the sum of all particle-hole diagrams,[33] and the effective particle-hole interaction $\overline{U}$,[34,35]

$$\Phi^{\mathrm{SF}}=N(\phi_2+\phi_\perp+\phi_\parallel), \quad (2.17)$$

$$\phi_2=-\frac{1}{2}\beta^{-1}\overline{U}^2\sum_{\mu}\chi^{(0)}_{\uparrow\uparrow}(i\omega_\mu)\chi^{(0)}_{\downarrow\downarrow}(i\omega_\mu), \quad (2.18)$$

$$\phi_\perp=\beta^{-1}\sum_{\mu}\ln[1-\overline{U}\chi^{(0)}_{\uparrow\downarrow}(i\omega_\mu)]+\beta^{-1}\overline{U}\sum_{\mu}\chi^{(0)}_{\uparrow\downarrow}(i\omega_\mu)+\frac{1}{2}\beta^{-1}\overline{U}^2\sum_{\mu}\chi^{(0)}_{\uparrow\downarrow}(i\omega_\mu)\chi^{(0)}_{\downarrow\uparrow}(i\omega_\mu), \quad (2.19)$$

$$\phi_\parallel=\frac{1}{2}\beta^{-1}\sum_{\mu}\ln[1-\overline{U}^2\chi^{(0)}_{\uparrow\uparrow}(i\omega_\mu)\chi^{(0)}_{\downarrow\downarrow}(i\omega_\mu)]+\frac{1}{2}\beta^{-1}\overline{U}^2\sum_{\mu}\chi^{(0)}_{\uparrow\uparrow}(i\omega_\mu)\chi^{(0)}_{\downarrow\downarrow}(i\omega_\mu), \quad (2.20)$$

where

$$\chi^{(0)}_{\sigma\sigma'}(i\omega_\mu)=-\beta^{-1}\sum_{\nu}\mathcal{G}^0_{\mathbf{Q},\sigma}(i\omega_\nu)\mathcal{G}^0_{\mathbf{Q},\sigma'}(i\omega_\nu+i\omega_\mu) \quad (2.21)$$

is the noninteracting particle-hole susceptibility. Self-consistency would require that $\Phi^{\mathrm{SF}}=\Phi^{\mathrm{SF}}[G_{\mathbf{Q}}]$; here instead we apply the non-self-consistent procedure introduced by Bulut, Scalapino, and White,[36] and approximate $\Phi^{\mathrm{SF}}[G_{\mathbf{Q}}]\rightarrow\Phi^{\mathrm{SF}}[\mathcal{G}^0_{\mathbf{Q}}]$. It has been shown that this procedure may be regarded to be a reasonable approximation as the thermodynamic potential (2.13) is stationary and one expects not to move too far away from its minimum.

C. Self-energy with local spin fluctuation

It is known to be notoriously difficult to obtain an analytic expression for the self-energy, and so far an ansatz within the iterative perturbation scheme (IPS) based on SOPT has mostly been used.[22] The ansatz introduces an approximate form of self-energy which starts from the SOPT and allows one to reproduce the exact results in certain limits. Although this approach reproduces the correct large-U limit,[22] it overestimates the correlation effects in the nonmagnetic states, and thus becomes uncontrollable in the intermediate-U regime. Therefore, it cannot be applied to investigate the phase stability and dynamics in the magnetic states of the Hubbard model. We have verified that the AF LRO disappears in the 2D Hubbard model ($t'=t''=0$) at half-filling for $U\simeq 5t$ for $t'=t''=0$, if the formula introduced by Kajueter and Kotliar[22] is used (see Sec. IV A).

The SF part of the self-energy, $\Sigma^{\mathrm{SF}}_{\mathbf{Q}\sigma}(i\omega_\nu)$ follows from the Kadanoff-Baym potential (2.13) containing a class of diagrams up to infinite order:

$$\Sigma^{\mathrm{SF}}_{\mathbf{Q}\sigma}(i\omega_\nu)=\frac{\overline{U}^2}{\beta}\sum_{\mu}\chi_{\bar{\sigma}\bar{\sigma}\mathbf{Q}}(i\omega_\mu)\mathcal{G}^0_{\mathbf{Q}\bar{\sigma}}(i\omega_\nu-i\omega_\mu)+\frac{\overline{U}^2}{\beta}\sum_{\mu}\chi_{\bar{\sigma}\sigma,\mathbf{Q}}(i\omega_\mu)\mathcal{G}^0_{\mathbf{Q}\sigma}(i\omega_\nu-i\omega_\mu). \quad (2.22)$$

Here we approximated $\Sigma[G]$ by $\Sigma[\mathcal{G}^0]$ and avoid self-consistency. The transverse part in Eq. (2.22) resembles the self-energy derived by the coupling of the moving hole to transverse spin fluctuations, as derived using the spin-wave theory.[37] However, the longitudinal part is not included in

the latter approach, and we find that it cannot be neglected in the relevant regime of parameters for high temperature superconductors.

The self-energy in a magnetic system is calculated using the Weiss effective field (2.12) in the symmetry-broken magnetic state. The transverse,

$$\chi^{-}_{\sigma\sigma}(i\omega_\mu)=\overline{U}\frac{[\chi^{(0)}_{\sigma\sigma}(i\omega_\mu)]^2}{1-\overline{U}\chi^{(0)}_{\sigma\sigma}(i\omega_\mu)}, \tag{2.23}$$

and longitudinal,

$$\chi_{\sigma\sigma}(i\omega_\mu)=\frac{\chi^{(0)}_{\sigma\sigma}(i\omega_\mu)}{1-\overline{U}^2\chi^{(0)}_{\uparrow\uparrow}(i\omega_\mu)\chi^{(0)}_{\downarrow\downarrow}(i\omega_\mu)}, \tag{2.24}$$

susceptibilities in Eq. (2.22) are found in the random-phase approximation with renormalized interaction $\overline{U}$. Here the noninteracting susceptibilities $\chi^{(0)}_{\sigma\sigma}(i\omega_\mu)$ are calculated from the dynamical Weiss field Green function (2.12).

We would like to emphasize that the renormalized interaction $\overline{U}$ is not a fitting parameter,[36] but results from static screening by particle-particle diagrams, which leads to[34,35]

$$\overline{U}=U/[1+U\chi^{pp}(0)], \tag{2.25}$$

where the particle-particle vertex is again determined by the Weiss field,

$$\chi^{pp}(0)=\beta^{-1}\sum_\mu \mathcal{G}^0_{\mathbf{Q}\uparrow}(i\omega_\mu)\mathcal{G}^0_{\mathbf{Q}\downarrow}(-i\omega_\mu). \tag{2.26}$$

This screening effect gives the magnetic structure factor[34] and the self-energy[36] calculated from Eq. (2.22) in good agreement with the QMC results, and depends on the underlying magnetic order. It is largest in the paramagnetic states and vanishes in the Néel state at $n=1$ for $U\to\infty$, and is thus very important when the magnetic phase diagrams are considered.[35] The proposed self-energy (2.22) expresses the spin-fluctuation exchange interaction[38] with an effective potential due to particle-particle scattering.[34]

Equations (2.11), (2.12), and (2.22) represent solutions for the one-particle Green function within DMFT. They have been solved self-consistently, and an energetically stable spiral configuration was found. This procedure is further justified by the sum rule[39]

$$\frac{1}{2\beta}\sum_{\nu\sigma}\Sigma_\sigma(i\omega_\nu)G_\sigma(i\omega_\nu)e^{i\omega_\nu 0^+}=U\langle n_{0\uparrow}n_{0\downarrow}\rangle, \tag{2.27}$$

which is well fulfilled in the present approach with $U\langle n_{0\uparrow}n_{0\downarrow}\rangle\simeq\overline{U}\langle n_{0\uparrow}\rangle\langle n_{0\downarrow}\rangle$.[35] We also show below (Sec. IV A) that the local self-energy (2.22) leads to an overall satisfactory agreement with QMC and ED data.

III. EXCITATION SPECTRA

A. Photoemission at finite temperature

A complete theory of photoemission (PES) would require an analysis not only of the one-particle Green's function but also of the three-particle Green's functions. We would like to point out that quantitative calculations of the three-particle Green's function for strongly correlated systems has not yet proven feasible. However, some aspects of the problem can be discussed in terms of the one-electron spectrum, provided that ''final-state'' or ''particle-hole'' interactions can be neglected. Under this assumption the problem simplifies, and the PES spectrum may be determined using the one-particle Green function alone. Such an approach which neglects final-state and particle-hole interactions has been applied with success to interpret[6] the dispersion found in the ARPES data of the copper oxides.[40,41]

Here we shall derive the relation of the PES spectra to the one-electron spectral function within the ''sudden'' approximation, where final-state interactions are neglected.[42] To be specific, let us consider a transition from a state $|n\rangle$ with energy E_n into a state of the form $A^\dagger_{\mathbf{k}\nu}|m\rangle$, in which we treat the photoelectron in state $|\mathbf{k}\nu\rangle$ as dynamically decoupled, but retain the full many-body interactions of the electrons in the bulk described by the Hubbard model Hamiltonian. The PES intensity for the magnetic system with an incommensurate magnetic order is nontrivial within the DMFT approach, as one cannot use a Bogoliubov transformation to establish the relation between the measured electrons and their local states in the SS state. The outgoing photoelectron is observed in the *global reference system*, whereas the quantum states of the bulk $|n\rangle$ have to be considered within the *local reference system* for the spin degrees of freedom. For clarity we write in the following the operators for the scattered states in capital letters, and the operators for the electronic states of the solid described by the present model Hamiltonian in lowercase letters.

At finite temperature T we consider the probability density of the absorption of a photon with frequency ω in a grand canonical ensemble, and obtain

$$\mathcal{W}(\mathbf{k},\omega)=Z^{-1}\sum_{mn} e^{-\beta K_n}|I^\nu_{mn}|^2\delta(\varepsilon_{\mathbf{k}}+K_m-K_n-\omega), \tag{3.1}$$

with $K_n\equiv E_n-\mu N_n$ and the partition function $Z=\Sigma_n e^{-\beta K_n}$. The amplitude of the transition,

$$I^\nu_{mn}=\langle m|A_{\mathbf{k}\nu}\sum_{\substack{\mathbf{p}\mathbf{p}'\\ \sigma\sigma'}} A^\dagger_{\mathbf{p}\sigma}[\Delta_{\mathbf{Q}}(\mathbf{p},\mathbf{p}')]_{\sigma\sigma'}c_{\mathbf{p}'-(\mathbf{Q}/2),\sigma'}|n\rangle, \tag{3.2}$$

is determined by the optical matrix element

$$\hat{\Delta}_{\mathbf{Q}}(\mathbf{p},\mathbf{p}')=\frac{1}{2}\Delta_{\mathbf{p},\mathbf{p}'}\left[\cos\frac{\theta}{2}(\hat{1}-\hat{\sigma}_z)+\sin\frac{\theta}{2}\hat{\sigma}_-\right] +\frac{1}{2}\Delta_{\mathbf{p},\mathbf{p}'-\mathbf{Q}}\left[\cos\frac{\theta}{2}(\hat{1}+\hat{\sigma}_z)-\sin\frac{\theta}{2}\hat{\sigma}_+\right], \tag{3.3}$$

and can be calculated using the Bloch wave functions in the *global reference system*,

$$\Delta_{\mathbf{p},\mathbf{p}'}=\tfrac{1}{2}\sum_\sigma\langle\Psi_{\mathbf{p}\sigma}|\boldsymbol{\epsilon}\cdot\mathbf{k}|\psi_{\mathbf{p}'\sigma}\rangle, \tag{3.4}$$

where $\boldsymbol{\epsilon}$ is the polarization vector. The operator $\mathbf{k}=-i\boldsymbol{\nabla}$ conserves total momentum in the scattering plane, so that

$\Delta_{\mathbf{p},\mathbf{p}'} \propto \delta_{\mathbf{p}_\parallel,\mathbf{p}'+\mathbf{K}}$, where $\mathbf{K}$ is a 2D lattice vector, and $\mathbf{p}_\parallel$ is the photoelectron momentum component in the 2D plane.

For solids the outgoing wave solution is the ''time-inverted low-energy electron diffraction (LEED) state.''[43] The LEED state consists of an incoming plane wave, reflected plane waves, and a combination of Bloch waves inside the solid which fulfill the matching boundary conditions. In lowest order we have one (damped) Bloch wave traveling away from the surface. In the time-inverted (complex conjugated) state the Bloch wave travels toward the surface, and goes over in a plane wave outside. The LEED scattered waves become incoming waves on time inversion, and give no contribution to the photocurrent. The photoelectron is usually detected at energies which are much higher than the typical energy regime described by the Hubbard model, and therefore the Bloch waves occupy high-energy quantum states which are initially unoccupied,

$$A_{\mathbf{k}\sigma}|n\rangle \simeq 0. \tag{3.5}$$

Hence for the plane SS state ($\theta=\pi/2$) we obtain

$$\mathcal{W}(\mathbf{k},\omega) = -\frac{1}{\pi}\sum_{\sigma\sigma'} |\Delta_{\mathbf{k},\mathbf{k}}|^2 n_{\mathrm{F}}(\epsilon_{\mathbf{k}}-\omega) \times \mathrm{Im}\, G_{\sigma\sigma'}(\mathbf{k}-\mathbf{Q}/2,\varepsilon_{\mathbf{k}}-\omega), \tag{3.6}$$

where $n_{\mathrm{F}}(\omega)$ is the Fermi function, and the following identity, valid only for plane spirals ($\theta=\pi/2$), has been used ($\lambda_\sigma=1,-1$ for $\sigma=\uparrow,\downarrow$);

$$\sum_{\sigma\sigma'} G_{\sigma\sigma'}(\mathbf{k}-\mathbf{Q}/2,\omega) = \sum_{\sigma\sigma'} \lambda_\sigma \lambda_{\sigma'} G_{\sigma\sigma'}(\mathbf{k}+\mathbf{Q}/2,\omega). \tag{3.7}$$

Within the ''sudden'' approximation the measured PES spectra near the Fermi energy can therefore be related to the one-electron spectral function [Eq. (3.6)] of the system with local spin-quantization axes, defined by

$$\mathrm{Im}\, G_{\sigma\sigma'}(\mathbf{k},\omega) = -\frac{\pi}{Z n_{\mathrm{F}}(\omega)}\sum_{mn} \langle n|c^\dagger_{\mathbf{k}\sigma'}|m\rangle \times \langle m|c_{\mathbf{k}\sigma}|n\rangle e^{-\beta K_n}\delta(\omega-K_n+K_m) \tag{3.8}$$

Therefore, the total one-particle excitation spectra is described by the spectral function

$$A(\mathbf{k},\omega) = -\frac{1}{\pi}\sum_{\sigma\sigma'} \mathrm{Im}\, G_{\mathbf{Q},\sigma\sigma'}\left(\mathbf{k}-\frac{\mathbf{Q}}{2},\omega+i\epsilon\right), \tag{3.9}$$

where $G_{\mathbf{Q},\sigma\sigma'}(\mathbf{k}-\mathbf{Q}/2,\omega+i\epsilon)$ is given by Eq. (2.11), and a numerical broadening $\epsilon>0$. The electron occupation number $\langle n_{\mathbf{k}}\rangle$ normalized per one spin, equal to the one-electron removal sum, can be obtained without analytic continuation of the Matsubara Green's function (2.11) by performing a direct summation over the Matsubara frequencies,

$$\langle n_{\mathbf{k}}\rangle = \frac{1}{2\beta}\sum_{\nu,\sigma\sigma'} e^{i\omega_\nu 0^+} G_{\mathbf{Q},\sigma\sigma'}\left(\mathbf{k}-\frac{\mathbf{Q}}{2},i\omega_\nu\right). \tag{3.10}$$

Finally, we also calculate the total densities of states in the AF and SS states using the derived spectral functions (3.9),

$$N(\omega) = \frac{1}{N}\sum_{\mathbf{k}} A(\mathbf{k},\omega). \tag{3.11}$$

B. Optical conductivity

We derived the complex optical conductivity $\sigma_{xx}(\omega)$ for the spiral magnetic order following the formalism introduced by Shastry and Sutherland,[44] and by Scalapino, White, and Zhang.[45] Their derivation has to be generalized to the case of extended hopping. Moreover, as the symmetry is locally broken in a magnetic system with local quantization axes, the calculation of the optical conductivity is not straightforward. The Hubbard Hamiltonian (2.4) within the local reference system for the spin quantization axis and first-, second-, and third-nearest-neighbor hopping elements, $t_{il}=t,\ t',$ and t'', respectively, has an electron kinetic energy

$$K = -\sum_{il,\sigma\sigma'}{}' t_{il}\{c^\dagger_{i\sigma}[\mathcal{R}^\dagger(\Omega_i)\mathcal{R}(\Omega_l)]_{\sigma\sigma'}c_{l\sigma'} + c^\dagger_{l\sigma'}[\mathcal{R}^\dagger(\Omega_l)\mathcal{R}(\Omega_i)]_{\sigma'\sigma}c_{i\sigma}\}, \tag{3.12}$$

where Σ'_{il} indicates a restricted sum, with $\mathbf{R}_l=\mathbf{R}_i+\|i-l\|_x\mathbf{x}+\|i-l\|_y\mathbf{y}$ around a given lattice site i, and $\mathbf{x}=(1,0)$, $\mathbf{y}=(0,1)$ are unit lattice vectors. We introduce a directed ''bond metric'' $\|i-l\|_{x(y)}$, which is a distance between two sites, i and l, *on the lattice*, and counts the number of $x(y)$-oriented bonds that connect site i with site l, respectively, e.g., $\|i-l\|_x=2$ and $\|i-l\|_y=0$ if the electron hops to a third-nearest-neighbor with amplitude t'' along an x-oriented link. Here $\mathcal{R}(\Omega_i)$ is the unitary matrix which transforms the original fermions $\{a^\dagger_{i\uparrow},a^\dagger_{i\downarrow}\}$ into the fermions quantized with respect to local quantization axes at each site, $\{c^\dagger_{i\uparrow},c^\dagger_{i\downarrow}\}$, introduced in Eq. (2.3). In what follows we are interested in the current response to a vector potential along the x direction of the 2D square lattice $A_x(l,t)$. In the presence of a vector potential, the hopping term is modified by the Peierls phase factor,[45] either $\exp\{+ieA_x(l,t)\|i-l\|_x\}$ or $\exp\{-ieA_x(l,t)\|i-l\|_x\}$, for t_{il} or t_{li}, respectively. Expanding these phase factors in the usual manner up to second order $\sim A^2$, one finds

$$K_A = K - \sum_{il}{}'\left[ej_x^P(i-l)A_x(l)+\frac{e^2}{2}k_x(i-l)A_x(l)^2\right]. \tag{3.13}$$

Here $j_x^P(i-l)$ is the x component of the paramagnetic current density,

$$j_x^P(i-l) = i\sum_{\sigma\sigma'}\|i-l\|_x t_{il}\{c^\dagger_{i\sigma}[\mathcal{R}^\dagger(\Omega_i)\mathcal{R}(\Omega_l)]_{\sigma\sigma'}c_{l\sigma'} - c^\dagger_{l\sigma'}[\mathcal{R}^\dagger(\Omega_l)\mathcal{R}(\Omega_i)]_{\sigma'\sigma}c_{i\sigma}\}, \tag{3.14}$$

and $k_x(i-l)$ is the kinetic-energy contribution due to the $x-$oriented links, weighted by the metric factor connecting site i with site l,

$$k_x(i-l) = -\sum_{\sigma\sigma'} \|i-l\|_x^2 t_{il}\{c^\dagger_{i\sigma}[\mathcal{R}^*(\Omega_i)\mathcal{R}(\Omega_l)]_{\sigma\sigma'} c_{l\sigma'} + c^\dagger_{l\sigma'}[\mathcal{R}^*(\Omega_l)\mathcal{R}(\Omega_i)]_{\sigma'\sigma} c_{i\sigma}\}. \quad (3.15)$$

After performing a Fourier transformation one finds the average contribution of kinetic energy (3.15) per one site,

$$\langle k_x\rangle = \frac{1}{N}\sum_{\mathbf{k},\sigma\sigma'} \langle c^\dagger_{\mathbf{k}\sigma}[\hat{t}_{x,\mathbf{Q}}(\mathbf{k})]_{\sigma\sigma'} c_{\mathbf{k}\sigma'}\rangle, \quad (3.16)$$

with the coupling between the transformed elements at momenta $\mathbf{k}-\mathbf{Q}/2$ and $\mathbf{k}+\mathbf{Q}/2$ due to the magnetic order,

$$\hat{t}_{x,\mathbf{Q}}(\mathbf{k}) = \frac{1}{2}\varepsilon_x\left(\mathbf{k}-\frac{\mathbf{Q}}{2}\right)(\hat{1}+\hat{\sigma}_z\cos\theta-\hat{\sigma}_x\sin\theta) + \frac{1}{2}\varepsilon_x\left(\mathbf{k}+\frac{\mathbf{Q}}{2}\right)(\hat{1}-\hat{\sigma}_z\cos\theta+\hat{\sigma}_x\sin\theta), \quad (3.17)$$

and $\varepsilon_x(\mathbf{k}) = -2t\cos k_x - 4t'\cos k_x\cos k_y - 8t''\cos 2k_x$.

As usual, the optical conductivity in long-wavelength limit $\mathbf{q}\to 0$, $\sigma_{xx}(\omega)=\sigma'_{xx}(\omega)+i\sigma''_{xx}(\omega)$, is determined by the current response to a vector potential along the x direction,[45] and one finds using the Kubo linear-response theory

$$\sigma_{xx}(\omega) = -e^2\frac{\langle -k_x\rangle - \Lambda_{xx}(\mathbf{q}=\mathbf{0},\omega+i0^+)}{i(\omega+i0^+)}, \quad (3.18)$$

where $\Lambda_{xx}(\mathbf{q},i\omega_\mu)$ is the current-current correlation function,

$$\Lambda_{xx}(\mathbf{q},i\omega_\mu) = \frac{1}{N}\int_0^\beta d\tau e^{i\omega_\mu\tau}\langle j_x(\mathbf{q},\tau) j_x(-\mathbf{q},0)\rangle. \quad (3.19)$$

The latter correlation function is given exactly by the particle-hole bubble diagram,[27,29] where, for $\mathbf{q}\to 0$,

$$j_x = \sum_{\mathbf{k},\sigma\sigma'} c^\dagger_{\mathbf{k}\sigma}[\hat{j}_{x,\mathbf{Q}}(\mathbf{k})]_{\sigma\sigma'} c_{\mathbf{k}\sigma'}, \quad (3.20)$$

and for the present SS state,

$$\hat{j}_{x,\mathbf{Q}}(\mathbf{k}) = \frac{1}{2}j_x\left(\mathbf{k}-\frac{\mathbf{Q}}{2}\right)(\hat{1}+\hat{\sigma}_z\cos\theta-\hat{\sigma}_x\sin\theta) + \frac{1}{2}j_x\left(\mathbf{k}+\frac{\mathbf{Q}}{2}\right)(\hat{1}-\hat{\sigma}_z\cos\theta+\hat{\sigma}_x\sin\theta), \quad (3.21)$$

with $j_x(\mathbf{k}) = 2t\sin k_x + 4t'\sin k_x\cos k_y + 4t''\sin 2k_x$. The advantage of using DMFT with the local self-energy is that the vertex corrections to the current-current correlation function (3.19) disappear, and the optical conductivity can be calculated without further approximations.[27]

We have verified for large variety of doping levels and temperatures that the optical sum rule

$$2\int_0^\infty d\omega\,\sigma'_{xx}(\omega) = e^2\pi\langle -k_x\rangle \quad (3.22)$$

is always fulfilled within the numerical accuracy, in contrast to the approaches which cannot be derived in a diagrammatic way. Equation (3.22) is also used to define the plasma-frequency ω_p,

$$\omega_p^2 = 8\int_0^\infty d\omega\,\sigma'_{xx}(\omega). \quad (3.23)$$

For the discussion of the complex conductivity function, it is convenient to introduce the following parametrization by the scattering rate, $\tau(\omega)^{-1}$, and the effective mass $m^*(\omega)/m_e$ (m_e is the electron mass):[46]

$$\sigma_{xx}(\omega) = \frac{\omega_p^2}{4\pi}\frac{1}{\tau^{-1}(\omega) - i\omega\dfrac{m^*(\omega)}{m_e}}. \quad (3.24)$$

From the real part of the optical conductivity [Eq. (3.18)], we find, in the limit $\omega\to 0$, the static conductivity

$$\sigma'_{xx}(\omega=0) = e^2\pi D + e^2\lim_{\omega\to 0}\frac{1}{\omega}\mathrm{Im}\,\Lambda_{xx}(\mathbf{q}=0,\omega), \quad (3.25)$$

with the Drude weight D which may be obtained from the zero-temperature extrapolation of the current-current correlation function in the upper complex plane,[45]

$$D = \lim_{T\to 0}[\langle -k_x\rangle - \mathrm{Re}\,\Lambda_{xx}(\mathbf{q}=0,2\pi iT)]. \quad (3.26)$$

The optical conductivity allows us to determine the in-plane static resistivity

$$\rho_{xx}(T) = \sigma'_{xx}(\omega=0,T)^{-1}, \quad (3.27)$$

where the static conductivity $\sigma'_{xx}(\omega=0,T)^{-1}$ is obtained as in Eq. (3.25). We present the results obtained for the optical conductivity and static resistivity in Sec. V, and show that the magnetic order in the doped compounds has directly measurable consequences for these quantities.

IV. ONE-PARTICLE SPECTRA

A. Quasiparticles at half-filling

The ground state of the Hubbard model with nearest-neighbor hopping ($t'=t''=0$) on a square lattice is an AF insulator. The insulating behavior and the gap develop gradually at half-filling with increasing U starting from $U=0$ due to the perfect nesting instability, leading to a Slater gap. This gap changes into a Mott-Hubbard gap under increasing U, and the system approaches the limit of a Heisenberg antiferromagnet.[47] This regime of large U was found to be difficult for a quantitative description within DMFT approaches,[19] as an accurate determination of the energy gains due to AF long-range order is there of crucial importance. Therefore, the attempts to describe the AF order based on the SOPT within the IPS failed and the magnetic order disappeared at larger U.[22] In contrast, the QMC calculation in the $d\to\infty$ limit gave a stable AF state for large $U>4t$.[20,48]

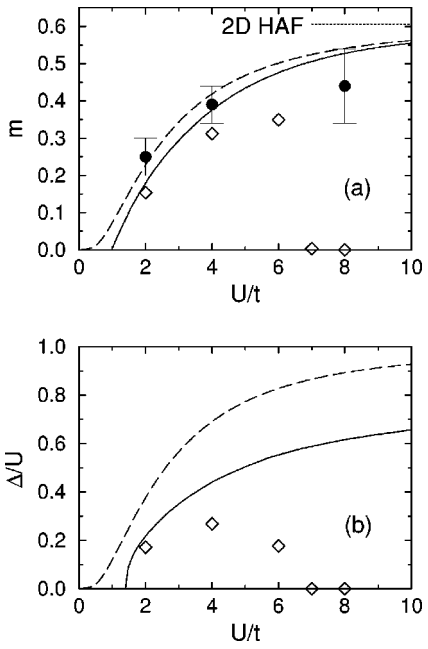

FIG. 1. Antiferromagnetic state for the Hubbard model at $n=1$: (a) magnetization m (4.1), and (b) the AF gap Δ/U in the 2D Hubbard model, as obtained using the HF approximation at $T=0$ (dashed lines) and the DMFT approach at $T=0.05t$ (full lines). The data points in (a) are QMC results reproduced from Ref. 51. The diamonds show the results of the IPS with the self-energy calculated in SOPT.

Here we treat the range of large $U \simeq W$ $(W=8t)$ as a test case for our analytic method. The calculations were performed at a low temperature $T=0.05t$ which allows one to describe the magnetic excitations $(T \ll J=4t^2/U)$. They gave an AF ground state at $n=1$, which reproduces correctly the localization of electrons in the limit of $U \to \infty$. The magnetization m_0 (2.2) is only slightly reduced by the dynamical effects with respect to its HF value, and approaches the HF limit at $U \to \infty$. The ground state is the Néel AF state, as found in the $d \to \infty$ limit.[49] Thus, we reduced the self-consistently obtained values of the mean-field magnetization m_0 (2.2) by a factor 0.606 in order to simulate the known reduction of m_0 by intersite quantum fluctuations in a 2D lattice,[50]

$$m = 0.606 m_0 . \tag{4.1}$$

After this reduction the calculated values of m approach the value of 0.606 in the limit $U \to \infty$ [Fig. 1(a)]. One finds also a very good agreement with the QMC data[51] at $U/t=2$ and 4, and a reasonable agreement at $U/t=8$.

In contrast, the AF gap Δ is significantly reduced from its HF value [Fig. 1(b)]. This reduction follows from a drastic change of the one-particle spectra by dynamical effects, which lead to QP states at the edge of the Mott-Hubbard gap which are accompanied by a large incoherent part at higher energies. Also the reduction of the gap found in ED (Ref. 52), comes out correctly, as shown in Ref. 24. For example, we found a gap of $4.93t$ at $U/t=8$, while the corresponding gap in the HF calculation is $7.14t$. This gap reduction can also be captured by the leading dynamical correlations described within the SOPT, but only in the regime of U

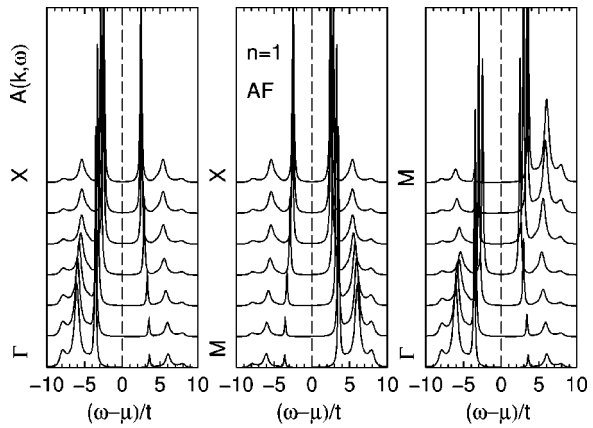

FIG. 2. One-particle excitation spectra as obtained in the AF state at $n=1$ and $T=0.05t$ for the Hubbard model with $U=8t$ $(t'=t''=0)$.

$<2.5t$. The discrepancy between SOPT and DMFT results increases with increasing U, with the gap and the magnetization m being too small, and finally the AF order disappears and the gap closes at $U \simeq 7t$. This shows the very limited applicability of approaches using the self-energy based on the SOPT,[22] which are known to underestimate the region of stability of magnetic states and fail at large U due to the uncontrolled increase of the correlation energy in nonmagnetic states.

The spectral functions found within the DMFT [Eq. (3.9)] are dominated by the lower Hubbard band (LHB), i.e., PES part at $\omega < \mu$, and the upper Hubbard band (UHB), i.e., inverse photoemission (IPES) part at $\omega > \mu$, separated by a large gap (Fig. 2). Both the PES and IPES spectrum show two distinct energy regimes: (i) narrow QP peaks at low energies, i.e., at the edge of the Mott-Hubbard gap; and (ii) incoherent and more extended features at higher energies $|\omega| > 5t$. The overall shape of the density of states $N(\omega)$ agrees very well with the ED data for a 4×4 cluster.[52] The spectra have a characteristic $\mathbf{k}$ dependence with the overall weight moving from the PES to IPES part along the Γ-X-M and Γ-M directions, where $\Gamma=(0,0)$, $X=(\pi,0)$ and $M=(\pi,\pi)$, in qualitative agreement with QMC data.[53] The spectra obey the particle-hole symmetry of the model, with spectra symmetric with respect to $\omega=0$ at the X and $S=(\pi/2,\pi/2)$ points. The spectrum at the M point is a mirror image of the one at the Γ point.

The QP maxima near the Mott-Hubbard gap resemble those found in the t-J model in ED or within the self-consistent Born approximation,[5] in spite of using a local self-energy in the present scheme. This shows that the local many-body problem solved within DMFT suffices to capture the low-energy scale relevant for the QP propagation. Moreover, unlike in the t-J_z model, which results in the ladder spectrum for a single hole,[54,55] the QP's *can propagate*, as they couple to the spin flips of the mean-field bath around site $i=0$ at which the many-body problem is being solved. The QP dispersion is $\sim 2J$ [Fig. 3(a)], with the maxima along the AF Brillouin zone (BZ), and remains very close to that found in the t-J model.[5]

In the HF approximation, the electron occupation factors $\langle n_{\mathbf{k}} \rangle$ are larger for the states which belong to the AF BZ than for the remaining states outside the AF zone. On comparing

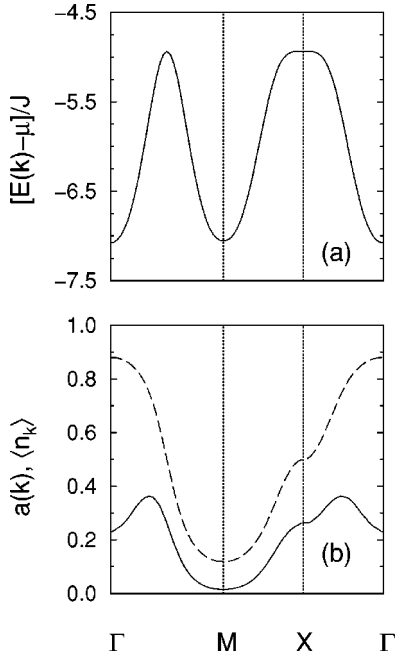

FIG. 3. Momentum dependence in the main directions of the 2D BZ, as obtained for the PES spectrum of the Hubbard model at half-filling with $t'=t''=0$, $U=8t$, and $T=0.05t$: (a) QP dispersion $[E(\mathbf{k})-\mu]/J$; (b) total electron occupation $\langle n_{\mathbf{k}}\rangle$ (dashed line) and QP weight $a(\mathbf{k})$ (full line).

the weights of the electronic states with momenta $\mathbf{k}$ and $\mathbf{k}+\mathbf{Q}$, one finds that also in the DMFT the electron weights are much larger within than outside of the AF BZ [Fig. 3(b)]. The overall PES weight is smoothly distributed in the 2D BZ, with the maximum (minimum) at the Γ (M) point, respectively. This result agrees well with a QMC simulations, and the present data show the same steplike behavior of the electron occupation factor $\langle n_{\mathbf{k}}\rangle$ when crossing the X point along the Γ-X-M direction as the QMC data at $U=4t$ and $8t$.[53,56]

A similar steplike behavior is also found in the QP weight $a_{\mathbf{k}}$ along the same line, determined by integrating the spectral functions (3.9) in an energy window of $2J$ which exhausts the range of the QP band in the density of states $N(\omega)$. The $\mathbf{k}$ dependence of the QP weight is more complex than that of $\langle n_{\mathbf{k}}\rangle$ as two competing effects contribute along the Γ-M and Γ-X directions when the Mott-Hubbard gap is approached: (i) the QP pole moves to lower energies and thus the weight increases; (ii) the overall PES weight is largest at the Γ point, and gradually decreases coming closer to the AF BZ. Therefore, the maxima in the QP weight are found close to $\mathbf{k}=(\pi/2,0)$ and between the Γ and $S=(\pi/2,\pi/2)$ points, while the (identical) weights at the X and S points are lower. The lowest QP weight is found at the M point, but here instead a distinct QP exists in the IPES part, in agreement with ED results.[57]

The QP weights $a(\mathbf{k})$ increase with increasing J/t and agree surprisingly well with the self-consistent Born approximation and ED data for the t-J model in the regime of $J/t<0.7$, as shown in Fig. 4. The average weight first increases somewhat faster than the numerical results of Ref. 55, but then flattens out above $J/t\simeq 0.6$, and saturates indicating that the t-J model does not represent faithfully the hole dynamics

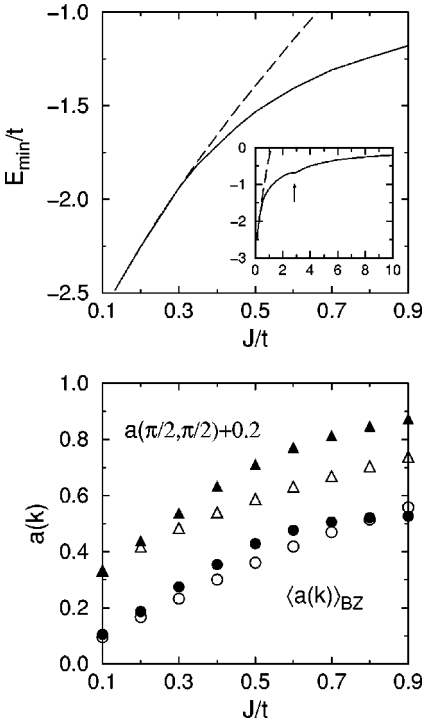

FIG. 4. Quasiparticles in the AF state at $n=1$: the minimum of the QP band $E_{\min}/t$ (upper part), and the QP weight $a(\mathbf{k})$ at $\mathbf{k}=(\pi/2,\pi/2)$ and averaged over the BZ (lower part) as functions of J/t. Filled and empty symbols stand for $a(\mathbf{k})$ found in the present DMFT approach and in the SCBA of Ref. 55. The inset in the upper part shows $E_{\min}/t$ for $0<J/t<10$; the value of J/t at which the AF order vanishes is indicated by an arrow.

in the Hubbard model at larger values of J/t, where the excitations to the UHB become important. An equally good agreement between the self-consistent Born approximation and ED data and the present DMFT approach is found at individual $\mathbf{k}$ points; the values of $a(\pi/2,\pi/2)$ are shown in Fig. 4, while a very good agreement with ED data at the X point was presented earlier in Ref. 24.

The energy at the minimum of the polaron band found at the S point follows the power-law behavior found by Martínez and Horsch[55] in the range of $J/t<0.4$ (Fig. 4),

$$\frac{E_{\min}(\mathbf{k}_S)}{t}=-3.20+2.94\left(\frac{J}{t}\right)^{0.702}. \tag{4.2}$$

This power law supports the string picture, but is again closer to the full single-hole problem in the t-J model, where the data obtained from finite cluster diagonalization could be fitted to the relation $E_{\min}/t=-3.17+2.93(J/t)^{0.73}$ (see Ref. 58) than to the t-J_z model, which gives instead $E_{\min}/t=-2\sqrt{3}+2.74(J_z/t)^{2/3}$ (see Ref. 59). It is also quite close to the exact solution of the t-J model in the infinite-dimensional lattice, given by $E_{\min}/t=-4+2.34(J/t)^{2/3}$, which interpolates to the Nagaoka state.[25]

Finally, we comment on the modifications of the spectra introduced by the changes in the parameters U and t_{ij}. Realistic parameters for $La_{2-x}Sr_xCuO_4$ and $YBa_2Cu_3O_{6+x}$ were estimated using both the cell method in the multiband charge-transfer model,[4] and the down-folding procedure in the electronic structure calculations.[7] Here we use the latter

TABLE I. Values of the model parameters used for the presented calculations; the parameter sets chosen for $La_{2-x}Sr_xCuO_4$ and $YBa_2Cu_3O_{6+x}$ follow from the down-folding procedure of Ref. 7.

Model parameters	t'/t	t''/t	U/t	J/t
Hubbard model	0.0	0.0	8.0	0.50
$La_{2-x}Sr_xCuO_4$	−0.11	0.04	10.0	0.40
$YBa_2Cu_3O_{6+x}$	−0.28	0.18	12.0	0.33

parameters as given in Table I, but the sets do not differ significantly. By increasing the value of U, one comes closer to the limit of the Heisenberg model, and therefore the momentum density $\langle n_{\mathbf{k}}\rangle$ is more uniformly distributed over the BZ [Fig. 5(b)]. This quantity depends mainly on the ratio of U/t, and thus a similar result is obtained at the same value of U with t' and t'' nonzero.

In contrast, the earlier studies of the t-t'-t''-J model have shown that the dispersion of QP's at low energy are strongly dependent on the values of the extended hopping parameters, t' and t''.[6] This strong dependence is also found in the present calculations based on the DMFT approach; the QP's at the S and X points are not degenerate any more as soon as $t'\neq 0$. Here we present only the representative result for larger values of $t'=-0.28t$ and $t''=0.18t$ found in $Sr_2CuO_2Cl_2$, with minima located close to the X point [Fig. 5(a)]. Although the QP weight is dominated by the same competition between the overall PES weight $\langle n_{\mathbf{k}}\rangle$ and the position of the QP maximum with respect to the Fermi level, the consequences of sizable $t'=-0.28t$ are clearly visible: the QP weight at the X point is reduced, and the degeneracy of the QP energies found before along the Γ-M and X-Γ directions [Fig. 3(b)], respectively, is now removed. As before, the lowest QP weight is found at the M point, and a distinct QP exists in the IPES part. Unlike at $t'=t''=0$, the latter IPES spectrum is different from the PES spectrum at the Γ point since there is no particle-hole symmetry at finite t'.

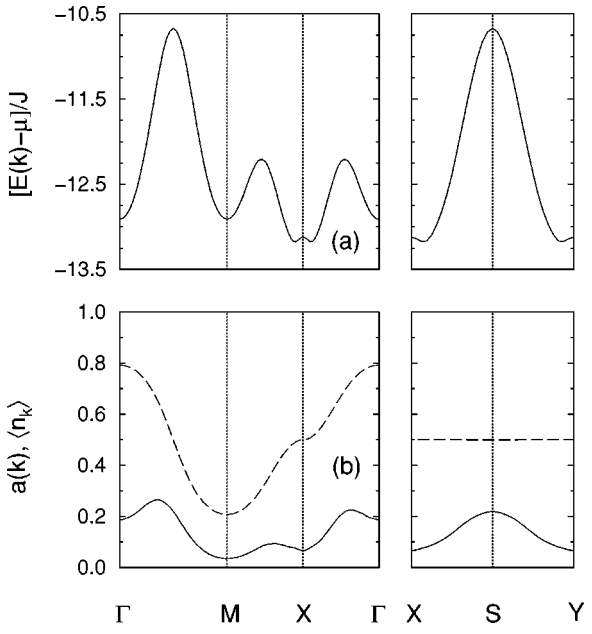

FIG. 5. Momentum dependence in the main directions of the 2D BZ, as obtained for the PES spectrum of the Hubbard model at half-filling with extended hopping parameters $t'=-0.28t$, $t''=0.18t$, $U=12t$, and $T=0.05t$: (a) QP dispersion $[E(\mathbf{k})-\mu]/J$; (b) total electron occupation $\langle n_{\mathbf{k}}\rangle$ (dashed line) and QP weight $a(\mathbf{k})$ (full line).

TABLE II. Values of magnetization m_0 (2.2) and the renormalized interaction $\bar{U}$ (2.25), as obtained for the Hubbard model ($t'=t''=0$) at $T=0.05t$, $\delta=1-n$, for different magnetic states: antiferromagnetic (AF), spin spiral [SS(1,1) and SS(1,0)], and paramagnetic (PM) states.

Ground state	δ	U/t	m_0	$\bar{U}/U$
AF	0.0	8	0.871	0.899
AF	0.125	8	0.689	0.755
SS(1,1)	0.125	8	0.675	0.735
SS(1,0)	0.125	8	0.657	0.733
AF	0.250	8	0.390	0.491
SS(1,1)	0.250	8	0.571	0.614
SS(1,0)	0.250	8	0.525	0.589
PM	0.125	8	0.0	0.327
PM	0.125	4	0.0	0.494

B. Spectral properties in spin-spiral states

As suggested by earlier studies,[11–17] hole doping away from half-filling leads to incommensurate magnetic order. We found the same sequence of spiral phases with increasing doping as in the HF and slave-boson calculations:[14,16] the AF order changes first into the SS with $\mathbf{Q}=[\pi(1\pm 2\eta),\pi(1\pm 2\eta)]$ along the (1,1) direction [the SS(1,1) state], and then at higher doping into the SS with $\mathbf{Q}=[\pi(1\pm 2\eta),\pi]$ along the (1,0) direction [the SS(1,0) state, or an equivalent SS(0,1) state]. SS states with the components of the characteristic $\mathbf{Q}$-vector shifted by $\pm 2\eta$ are physically equivalent and have the same energy. At fixed doping δ one finds, however, these phase transitions at larger values of U in the present approach which includes local correlation effects, than in the effective single-particle theories.[14,16] This change of the phase diagram follows from the correlation effects which screen the value of U to $\bar{U}$ (2.25), and strongly depend on the magnetic order (Table II). The highest value of effective $\bar{U}/U$ is obtained in the AF state at half-filling, where the double occupancy is strongly reduced and the screening is thus ineffective. The screening is stronger in the doped cases, indicating that the moving electrons correlate and avoid each other, leading to much weaker effective repulsion, and is particularly pronounced in paramagnetic states. We found here a surprisingly good agreement for the effective interaction $\bar{U}=1.98t$ found at $U=4t$ with the fitted value of $\bar{U}=2t$ in the QMC calculations.[36]

Two regions of phase separation which follow from the Maxwell construction[14] were found for the Hubbard model at $U/t=8$ ($t'=t''=0$): a crossover regime from the AF to SS(1,1) state for $0<\delta<0.11$, and from the SS(1,1) to SS(1,0) state for $0.22<\delta<0.25$, respectively (Fig. 6). The value of the chemical potential μ is $U/2$ at half-filling, and drops abruptly at infinitesimal doping when it enters the

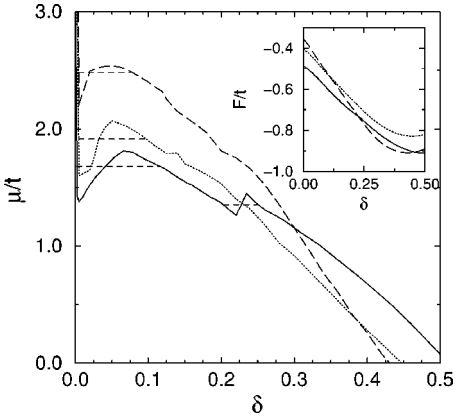

FIG. 6. Chemical potential μ/t as a function of doping δ, as obtained at $T=0.05t$ for three sets of parameters given in Table I: the Hubbard model with $U=8t$ (full line) and the model parameters of $La_{2-x}Sr_xCuO_4$ (dotted line) and $YBa_2Cu_3O_{6+x}$ (long-dashed line). The regions of phase separation obtained from the Maxwell construction are indicated by dashed lines. The inset shows the free energy F/t per site.

LHB in a doped system. The doping dependence of the free energy indicates a phase separation at low doping; this region becomes gradually narrower with increasing U, in agreement with other calculations.[60,61] In contrast, the transition to the SS(1,0) state moves to larger doping with increasing U, and finally disappears. Already at the model parameters of doped La_2CuO_4 we found no region of stable SS(1,0) state. It is worth noting, however, that in this case a small region of almost flat chemical potential μ was found for $\delta\simeq 1/8$ which could be considered as a precursor effect for the phase separation. It might lead to a different magnetic state at still lower temperatures,[13,60] as the stripe structures observed in the neutron experiments.[9]

The **k**-resolved spectral functions (Figs. 7 and 8) allow us to identify the generic features of the doped antiferromagnets described by the Hubbard model, in the regime of large U. First of all, the spectra are still dominated by the large *Mott-Hubbard gap* which separates the LHB from the UHB. The Mott-Hubbard gap develops from the respective gap at half-filling and is considerably reduced from U by the QP subbands which occur next to the large gap both in the LHB and in the UHB. This large gap is accompanied by a smaller *pseudogap* $\sim 2t$ between the occupied (PES) and unoccupied (IPES) part of the LHB at low temperature $T=0.05t$ (taking $t\simeq 0.4$ eV it corresponds to ~ 200 K). This pseudogap results from the SS order, and separates the majority and minority spin states (with respect to the local coordinates at each site). It is best visible along the Γ-X and X-M directions at $\delta=0.125$, and becomes somewhat wider and less distinct in the SS(1,0) spiral at higher doping $\delta=0.25$. We emphasize that the two features below and above the chemical potential μ originate from the same QP peak at half-filling. This shows that the QP found in the spectral function of one hole in the t-J (or Hubbard) model cannot describe the regime with finite doping as the *rigid band picture breaks down*.

The pseudogap is visible along the Γ-X direction starting from $\mathbf{k}=(\pi/2,0)$, and the maximum above the chemical potential μ grows gradually toward the X point. Consider first

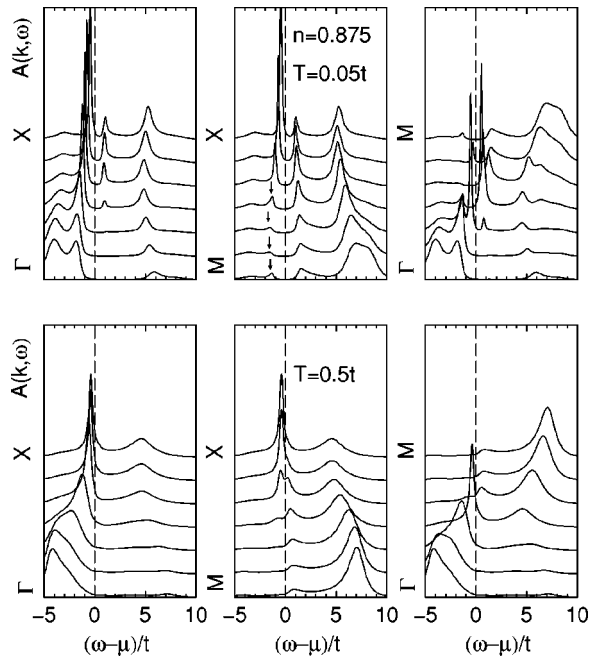

FIG. 7. Spectral functions $A(\mathbf{k},\omega)$ in the main BZ directions Γ-X, M-X, and Γ-M in the SS(1,1) state at $\delta=0.125$ and $U=8t$ for $T=0.05t$ (top) and $T=0.5t$ (bottom). The spectra along the Γ-M direction have been averaged over the (1,1) and $(\overline{1},\overline{1})$ spirals, defined by $\mathbf{Q}=\pi(1-2\eta)(1,1)$ and $\mathbf{Q}=\pi(1+2\eta)(1,1)$, respectively. A shadow band below μ in the M-X direction at $T=0.05t$ is indicated by arrows.

the case of lower doping $\delta=0.125$ (underdoped case). One finds that most of the spectral weight at the X point is still at $\omega<\mu$, with a sharp QP peak at $\omega\simeq -0.44t$. Increasing **k** along the X-M direction gives a transfer of the overall weight to higher energies, and the QP peak below μ gradu-

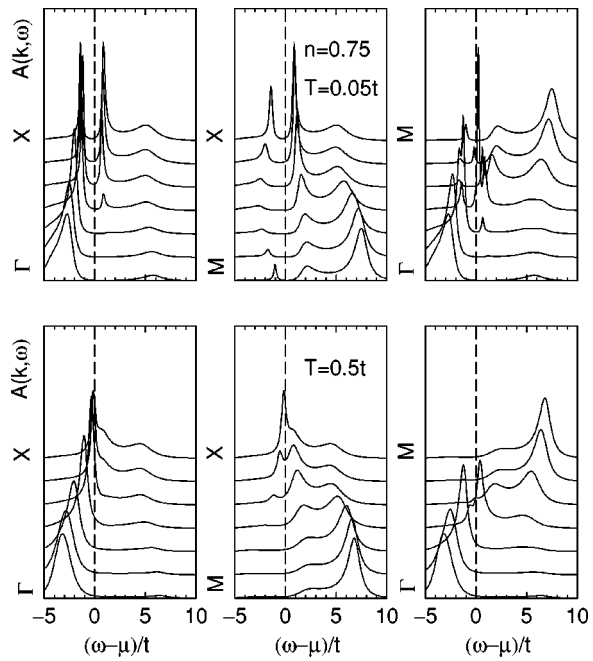

FIG. 8. Spectral functions $A(\mathbf{k},\omega)$ as in Fig. 7, but for $\delta=0.25$ and (1,0) spiral at $T=0.05t$. The conventions are the same as in Fig. 7.

ally loses intensity, while the peak above μ takes over around $\mathbf{k}=(\pi,\pi/3)$. However, the feature at $\omega<\mu$ is still well visible as a ''shadow'' QP band (Fig. 7), with a width $\sim 2J$. Thus the QP band of the t-J model is drastically modified at finite doping, and an energy scale $\sim 1.5t$ due to the pseudogap accompanies the dispersive QP feature below the chemical potential.

A similar situation is found also at higher doping $\delta=0.25$ (overdoped regime), and the pseudogap is quite pronounced along the Γ-X and X-M directions (Fig. 8). However, except for the neighborhood of the Γ point, more spectral weight is found at high energies. Already at the X point one finds that the peak at $\omega\simeq t$ has a higher intensity than the one below μ. It becomes gradually weaker when the M point is approached, and disperses in the energy range $\sim 3J$, while the feature below μ still has a similar dispersion $\sim 2J$ as in the $\delta=0.125$ case. We note that the pseudogap increases to $\sim 2.5t$. Moreover, one finds that the QP dispersion is broader at $\delta=0.25$, indicating the gradual weakening of the local magnetic order with increasing doping.

The spectra are drastically changed, in particular in the low-energy range of $|\omega-\mu|<2t$ when the temperature is increased. At $T\simeq 0.3t$ the SS order is unstable against the AF order which we interpret as a crossover to the small regions of the short-range order with the preferably AF ordering of nearest-neighbor spins. The spectra found for doping $\delta=0.125$ at $T=0.5t$ consist of broad maxima which correspond to the LHB and UHB, respectively, and only a single maximum is found in $A(\mathbf{k},\omega)$ next to the X point. These data, and also the spectral functions for $T=0.33t$ reported earlier,[24] agree remarkably well with the results of QMC calculations.[62] The spectra at $\delta=0.25$ and $T=0.5t$ are quite similar to those at lower doping $\delta=0.125$, with more weight in the IPES part of the LHB.

We do not intend to present a detailed analysis of the spectra obtained using the extended hopping parameters which correspond to the electronic structure of $La_{2-x}Sr_xCuO_4$ and $YBa_2Cu_3O_{6+x}$, respectively. Instead, we point out the important similarities and differences to the Hubbard model as far as the SS states are concerned. Consider first the effective parameters of $La_{2-x}Sr_xCuO_4$. First of all, a narrow QP band is also found below the Fermi energy (Fig. 9), but the measured dispersion between the Γ and X points is $\sim 0.80t$ ($\sim 2.56t$) at $\delta=0.125$ ($\delta=0.25$), while it amounts only to $\sim 0.36t$ at $\delta=0$. Note that the energies of the QP peak are much closer to each other for the present parameters than in the Hubbard model with $t'=t''=0$, where one finds instead the dispersion of $1.37t$ ($3.58t$) at $\delta=0.125$ ($\delta=0.25$) at $U=8t$, while it amounts to $1.1t$ in the undoped case. This gradual widening of the QP dispersion with increasing doping may be understood as a consequence of the admixture of ferromagnetic components with increasing doping in the SS(1,1) states. The same trend is also observed for the parameters of $YBa_2Cu_3O_{6+x}$, where one finds the QP states in the PES part separated by $\sim 0.39t$ ($\sim 1.94t$) between the Γ and X points at $\delta=0.10$ (0.25) (Fig. 10), while this splitting is only $\sim 0.07t$ at half-filling.

Finally, the finite hopping elements to the second and third neighbors also stabilize the SS(1,1) state with respect to the SS(1,0) state at higher doping (see Fig. 6), and therefore

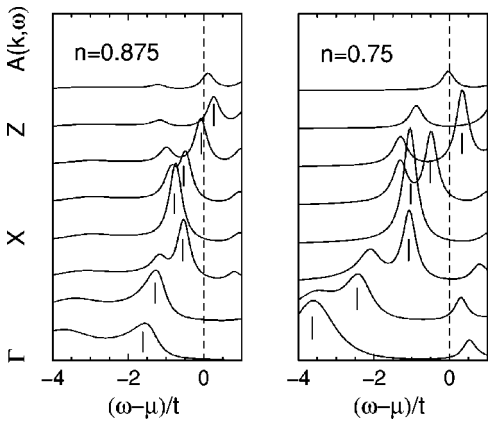

FIG. 9. Spectral functions $A(\mathbf{k},\omega)$ along the two main directions in a 2D BZ: Γ-X [with the step of $(\pi/3,0)$] and X-Z, where $Z=(\pi,\pi/2)$ [with the step of $(0,\pi/6)$], in SS(1,1) state as obtained for the model parameters of doped $La_{2-x}Sr_xCuO_4$ (Table I) at doping $\delta=0.125$ (left) and $\delta=0.25$ (right), and after averaging over all equivalent SS states with different values of $\mathbf{Q}$. The dispersive feature with the strongest intensity is indicated by vertical lines.

the intensity at the X point does not cross the Fermi level even at $\delta=0.25$ for both parameter sets. In fact, taking $J=0.125$ meV ($t/J=3$), the QP state at the X point is found at $\omega\simeq -0.56$ eV, and does not change significantly as a function of doping (Fig. 10). In contrast, in the ARPES experiments for $Bi_2Sr_2CaCu_2$ the QP state at X point is found at energy $\simeq -0.20$ eV ($\simeq -0.056$ eV) in the underdoped (optimally doped) compound.[40] This indicates that either an improved solution of the many-body problem is still required, or the actual magnetic order in these compounds might be different from SS states. However, the observed increase of the onset of incommensurability with increasing U and t' is consistent with the observations made by Igarashi and Fulde[17] and with QMC calculations of Duffy and Moreo.[63]

C. Total densities of states

We already pointed out[24] a very good agreement between the calculated density of states (3.11) and the results of ED

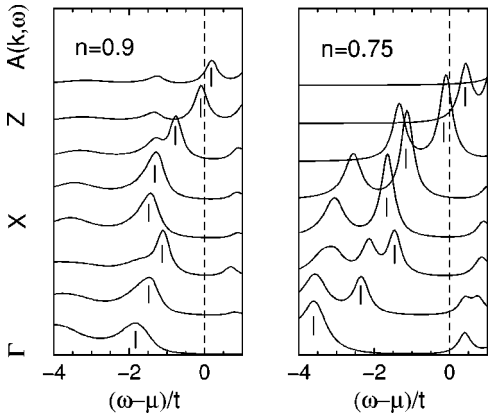

FIG. 10. The same as in Fig. 9, but for the model parameters of doped Y(Bi) superconductors (Table I) at dopings $\delta=0.10$ (left) and $\delta=0.25$ (right), and after averaging over all equivalent SS states with different values of $\mathbf{Q}$.

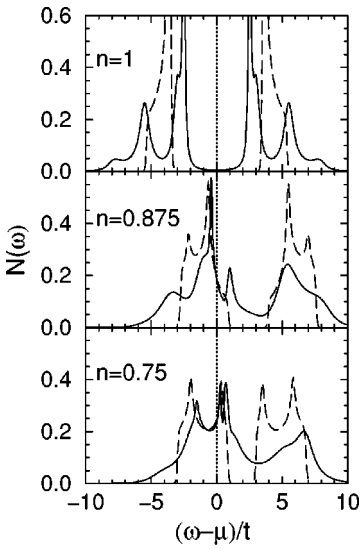

FIG. 11. Total densities of states $N(\omega)$ as obtained within DMFT (full lines) for $\delta=0$ (AF state), 0.125 [(1,1) spiral], and 0.25 [(1,0) spiral] with $U/t=8$ and $T=0.05t$. The dashed lines show $N(\omega)$ for the magnetic ground states found in the HF approximation.

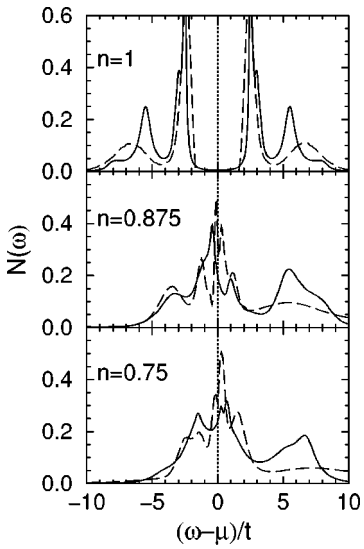

FIG. 12. Total densities of states $N(\omega)$ as obtained within DMFT at $U=8t$ by calculating the self-energy either using an analytic formula (2.22) (solid lines), or by DMFT-QMC method (dashed lines). Different panels show the results obtained for $\delta=0$ (AF state), 0.125 [(1,1) spiral], and 0.25 [(1,0) spiral], respectively, at $T=0.05t$.

by Dagotto *et al.*[52] Here we present instead a comparison between the density of states obtained within the DMFT method and that found in the HF approximation (Fig. 11). First of all, one notices a narrower gap of width $\sim 2J$ which separates the QP subbands in DMFT, instead of the HF one-particle states, on the scale of $\sim 2t$. This part of the spectral density might also be reproduced in effective single-particle approaches, as for instance in the slave-boson mean-field theory. However, the incoherent parts which extend on the energy scale down to $|\omega-\mu|\simeq 9t$ result from many-body scattering, and can only be reproduced if the dynamical part of the self-energy is included. The overall width of the subbands at $\omega<\mu$ and $\omega>\mu$ is $\sim 7t$, respectively, as known from the analysis of the t-J model in ED and in QMC calculations.[5]

It is evident that due to the changes of $N(\omega)$ in the range of $|\omega-\mu|\leqslant 1.5t$ with respect to the QP band in the undoped system, the low-energy part of the spectrum cannot be reproduced in a renormalized one-particle theory. The pseudogap in the doped systems is not visible in the HF densities of states, and it remains a challenge whether an effective one-particle theory which captures this essential new energy scale could be constructed. As expected, the agreement between the HF and DMFT densities of states improves somewhat at higher doping $\delta=0.25$, where the Mott-Hubbard gap is gradually lost, and the system approaches the single-particle limit. We note, however, that the gap between the LHB and UHB relies on magnetic order in our approach, and a more accurate approach in the strongly doped regime at large U would instead have to include the scattering on local moments.

In spite of very good agreement between the present DMFT approach and the ED data,[24] it is interesting to investigate to what extent the analytic formula for the self-energy (2.22) describes the hole dynamics in a doped system. Therefore, we also performed a DMFT-QMC calculation of local $\hat{\Sigma}_{\mathbf{Q}}(i\omega)$ for SS states, and the corresponding densities of states, shown in Fig. 12. The QP peaks are very close to each other at half-filling, while the incoherent states at higher energies in the LHB and UHB have almost the same weights, but are moved to somewhat higher energies in the QMC calculation. The increase of the spectral weight close to the Fermi level is well pronounced in the latter calculation at $\delta=0.125$, but one finds instead *a pseudogap smaller by a factor close to 5*. However, one should realize that the present calculation performed at low temperature $T=0.05t$ corresponds in practice to the ground state, while the same temperature in QMC already includes thermal fluctuations which considerably reduce the size of the pseudogap. Indeed, using the ED method to solve the self-energy within DMFT, we find a pseudogap in the SS state of $\sim 0.7t$. It might be expected that this reduction of the energy scale would result in a better quantitative description of the spectral functions and the related excitations across the pseudogap, leading to a reduced energy scale for the low-energy features of the optical conductivity (Sec. V). We also found a more extended energy range of the incoherent states which belong to the UHB in the QMC calculation. Altogether, the comparison with the DMFT-QMC calculation demonstrates that the analytic method developed in this paper is very useful to gain a qualitative insight into the possible changes of magnetic states under doping and their consequences for the properties measured in experiment.

V. OPTICAL AND TRANSPORT PROPERTIES

A. Optical conductivity in the Hubbard model

The evolution of the spectral functions $A(\mathbf{k},\omega)$ and the density of states $N(\omega)$ with doping, reported in Secs. IV A and III A, motivates an investigation of the optical properties. Here we make use of the theory introduced in Sec. III B,

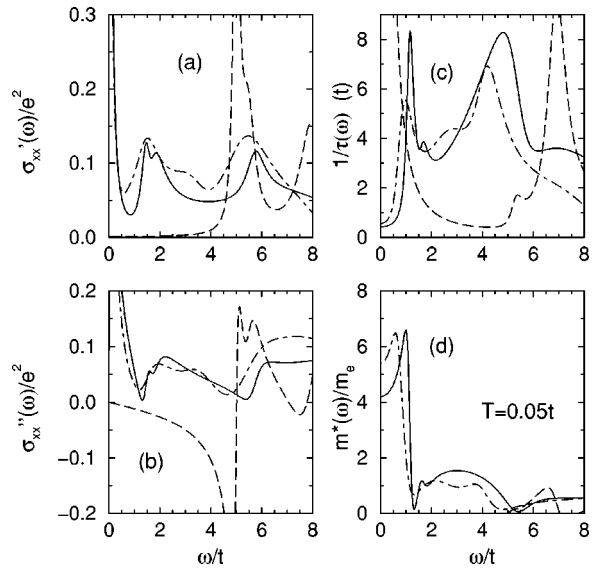

FIG. 13. Optical properties as functions of energy ω/t for the Hubbard model with $U=8t$ at low temperature $T=0.05t$ for $\delta=0$ (dashed lines), $\delta=0.125$ (full lines), and $\delta=0.25$ (dash-dotted lines): (a) real part of the optical conductivity $\sigma'(\omega)$; (b) imaginary part of the optical conductivity $\sigma''(\omega)$; (c) scattering rate $1/\tau(\omega)$; (d) effective mass $m^*(\omega)/m_e$.

where we have shown how the optical conductivity can be derived from the local self-energy in the present DMFT treatment.

As an illustrative example, we concentrate on the optical conductivity found for the Hubbard model with the nearest-neighbor hopping ($t'=t''=0$) and $U=8t$. We present the optical data in Figs. 13 and 14 at two temperatures: $T=0.05t$ and $0.2t$. While the magnetic order is AF at half-filling, the SS states characterized by the $\mathbf{Q}=[\pi(1\pm 2\eta_x),\pi(1\pm 2\eta_y)]$ wave-vector change with doping and temperature. At a lower doping $\delta=0.125$ we find a SS(1,1) with $\eta_x=\eta_y=0.125$ (0.09) at $T=0.05t$ ($T=0.2t$), respectively, while at higher doping $\delta=0.25$, a SS(1,0) state ($\eta_y=0$) with $\eta_x=0.25$ (0.23), or an equivalent SS(0,1) state, is found instead.

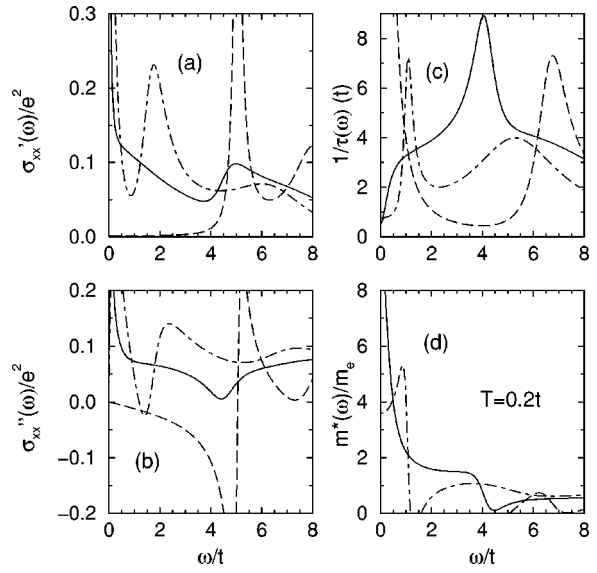

FIG. 14. Optical properties as functions of energy ω/t for the Hubbard model with $U=8t$ at intermediate temperature $T=0.2t$; the meaning of lines is as in Fig. 13.

At half-filling one finds a large gap below $\omega\simeq 4.9t$ at $U/t=8$ and no Drude peak, which shows that the system is in the insulating phase.[45] The conductivity at $\omega>4.9t$ is incoherent, and originates from excitations across the Mott-Hubbard gap. This changes drastically when the system is doped, and two new features occur at lower energy: the Drude peak and the midgap state at $\omega\simeq 2t$, both with increasing intensity between $\delta=0.125$ and 0.25 at low temperature (Fig. 13). These features are accompanied by an incoherent background of the excitations within the LHB. The peak at $\omega\simeq 2t$ corresponds to excitations across the pseudogap; as such it is more influenced by the increasing temperature in the underdoped regime, where the SS(1,1) state is less robust than the SS(1,0) state in the overdoped regime.

Below $\omega=4.9t$ the frequency dependent scattering rate $1/\tau(\omega)$ and the effective mass $m^*(\omega)/m_e$ can also be divided into two regions: (i) above $\omega\simeq 2t$ the scattering rate increases monotonically with increasing frequency; (ii) below $\omega\simeq 2t$ it has a maximum at energy $\omega\simeq 1.15t$ ($1.0t$) for $\delta=0.125$ (0.25), and drops to zero for $\omega\to 0$ at finite doping. This behavior for $\omega\to 0$ and $T\to 0$ is consistent with Fermi-liquid behavior, which follows from the local approximation to the self-energy (2.11). A finite value at $\omega=0$ is a numerical effect due to finite broadening of the spectra ($\epsilon=0.1t$).

The frequency region in which the scattering is suppressed has a direct relation to the existence of a pseudogap region in the single-particle spectral function $A(\mathbf{k},\omega)$, reported in Sec. IV B, and indicates that SS LRO reduces the scattering of the charged carriers in the energy range $\omega<1.15t$. At the same time, the effective mass $m^*(\omega)$ rises to a maximum value of $\sim 5m_e$ within the pseudogap region, and is found to be rather independent of hole doping. As the temperature increases to $T=0.2t$, the pseudogap disappears and the region of suppressed scattering is filled up in the underdoped regime with $\delta=0.125$, while the low scattering persists for $\omega<1.0t$ at $\delta=0.25$ (see Fig. 14). At the same time, the midgap state in the real part of the optical conductivity changes into a smooth feature which extends down to the Drude peak for $\delta=0.125$, contrary to the case with $\delta=0.25$, where the spectral weights of the above two features remain well separated. This is clearly related to the behavior observed in $A(\mathbf{k},\omega)$ with increasing temperature, where the pseudogap along the X-M direction filled up with spectral weight as T increased for $\delta=0.125$.

These changes of the midgap state with temperature are due to the changes of the magnetic correlations in the doped systems included in our calculations, which do not distinguish between long- and short-range magnetic orders, but treat local dynamical correlations. However, there are indications that the midgap feature results from an interplay between short-range magnetic order and electron correlations.[64] Therefore, the rather strong evolution of the low-energy weight with increasing temperature shown in Figs. 13 and 14 may be overestimated in the present treatment of the self-energy, which does not allow one to obtain a metal-insulator transition *without* an accompanying magnetic LRO. We also

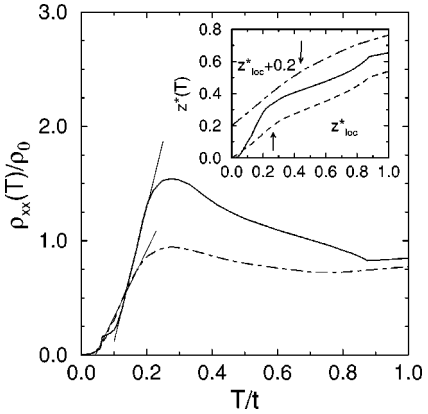

FIG. 15. Resistivity $\rho(T)/\rho_0$ as a function of temperature T/t as obtained for the Hubbard model with $U=8t$ for $\delta=0.125$ (full line) and $\delta=0.25$ (dashed line). The inset shows the weight $z^*(T)$ (5.1) found at the X point at $\delta=0.125$ (full line), and averaged weights over the Brillouin zone at $\delta=0.125$ (dashed line) and at $\delta=0.25$ (dash-dotted line). Arrows in the inset indicate T^*.

note that midgap states are likely a bare consequence of the strongly correlated nature of optical and one-particle excitations in the Hubbard model,[64] and it is still a challenge to describe them better in a theory which would treat the AF and paramagnetic states with local moments on equal footing.

The frequency-dependent scattering rate allows us to find a *crossover temperature* T^* at which the pseudogap closes. We estimated that $T^*\simeq 0.26t$ for $\delta=0.125$, and observed a monotonic increase of $1/\tau(\omega,T^*)$ up to $\omega\sim 4.1t$. At $T=0.2t$ the effective mass increases up to $\sim 10m_e$ within the pseudogap at $\delta=0.125$. At half-filling and $T=0.2t$, one finds that the charge-transfer gap is only slightly reduced from its value at $T=0.05t$, and the insulating behavior is accompanied by AF LRO. We estimated the Néel temperature for $U=8t$ to be $T_N\simeq 0.62J$.

Further evidence of a characteristic crossover temperature T^* may be found in the behavior of the in-plane dc resistivity (3.27). The resistivity has received a lot of attention in connection with the observed normal state pseudogap in the electronic excitation spectrum,[65] and from a theoretical point of view.[66,67] In fact, the physical origin of the linear T dependence of $\rho(T)$ for samples of high-T_c compounds close to the optimal doping level remains puzzling.

The results for $\rho_{xx}(T)$ obtained for the Hubbard model at two doping levels, $\delta=0.125$ and 0.25, are shown in Fig. 15. At low temperatures $T<0.06t$, the resistivity shows Fermi-liquid behavior for both hole densities, i.e., $\rho_{xx}(T)\propto T^2$. As usual in DMFT calculations,[67] the T^2 dependence of $\rho_{xx}(T)$ originates from the low-frequency behavior of the imaginary part of the local self-energy. In the regime of high temperatures ($T>0.9t$), the resistivity increases linearly with temperature which is due to temperature independence of the spectral functions $A_{\sigma\sigma'}(\mathbf{k},\omega)$ at $T\to\infty$, and the high temperature limit of the derivative $[(-\partial n_{\mathrm{F}}(\omega)/\partial\omega)\to 1/(4T)]$, thus leading to $\sigma_{xx}(T)\propto 1/T$, i.e., $\rho_{xx}(T)\propto T$. As the temperature is lowered, the magnetic moments gradually build up, and a kink in the resistivity appears. Therefore, the increase in the resistivity as the temperature is lowered can be attributed to an enhancement in the scattering of electrons by local spin fluctuations.

Conversely, for large hole doping the system is a better metal, hole spin correlations are gradually lost, and the increase of resistivity is less pronounced in the temperature region $T<0.88t$ at $\delta=0.25$. The maximum of $\rho_{xx}(T)$ for $\delta=0.125$ is located almost exactly at $T\approx 0.26t$ (~ 750 K taking the experimental value of the superexchange $J=125$ meV), where the pseudogap in the single-particle excitation spectra opens, leading to a suppression of the effective scattering rate $1/\tau(\omega,T)$, as discussed previously. This defines the crossover temperature T^*. Remarkably, the change from a linear to a nearly linear T dependence, $\rho_{ab}(T)\propto T^{1+\epsilon}$ ($\epsilon>0$), of the in-plane dc resistivity of $La_{2-x}Sr_xCuO_4$ was found to be at $T^*\simeq 600$ K for $x\simeq 0.13$, and was attributed to the opening of a pseudogap in the electronic excitation spectrum.[65] However, the saturation of the resistivity $\rho_{ab}(T)$ cannot be observed in a real system as the carriers also couple to other bosonic excitations, e.g., to phonons, which are neglected here.

Upon lowering the temperature below T^*, at $T<0.24t$ for both $\delta=0.125$ and 0.25, we observed a nearly linear T dependence of $\rho_{xx}(T)$. In this temperature range the SS wave vector, $\mathbf{Q}=[\pi(1\pm 2\eta_x),\pi(1\pm 2\eta_y)]$, becomes strongly temperature dependent, and maintains the directional deviation from the AF wave vector, $\mathbf{Q}_{\mathrm{AF}}=(\pi,\pi)$, with $\eta_x=\eta_y=\eta(T)$ for $\delta=0.125$ and $\eta_x=\eta(T)$ ($\eta_y=0$) for $\delta=0.25$. In both cases $\eta(T)$ increases from $\eta(T^*)\simeq 0$ with decreasing temperature, and saturates at its ground-state value $\eta(T=0)\simeq 2\delta$ below $T\simeq 0.08t$. In the linear regime ($T<T^*$) the resistivity can be fitted quite well by a linear T dependence, as expected for the SS states,[11] $\rho^{\mathrm{fit}}_{xx}(T)=\rho^{\mathrm{fit}}_{xx}(0)+\zeta\rho_0\delta^{-1}T$, with $\rho^{\mathrm{fit}}_{xx}(0)/\rho_0=-1.05$ (-0.25) for $\delta=0.125$ (0.25), respectively, where the increase of the negative temperature coefficient $\rho^{\mathrm{fit}}_{xx}(0)$ is a further manifestation of the gradual loss of local magnetic moments as doping is increased. Conversely, in the paramagnetic phase of the Hubbard model at $d=\infty$, one finds $\rho^{\mathrm{fit}}_{xx}(0)\geqslant 0$.[67] Furthermore, the slope of $\rho_{xx}(T)$ in the low-temperature regime is given by $\zeta\simeq 1.46$, independent of hole density. This value is larger by about a factor of 2.5 than the respective slope found in the retraceable-path approximation,[68] and in ED studies at finite temperature,[66] being $\zeta=0.55$ and 0.60, respectively, and demonstrates that the changes in the magnetic order with increasing temperature influence significantly the system resistivity. Unfortunately, such effects cannot be studied by the ED method due to the small size of the considered clusters.

In order to further support our observation that the crossover temperature T^* is related to the pseudogap in the single-particle excitation spectrum, in the inset of Fig. 15 we plot an average of the single-particle spectral weight within an energy window $\propto T$ around the Fermi energy $\omega=0$, defined by[69,39]

$$z^*(T)=-\sum_{\sigma\sigma'} G_{\sigma\sigma'\mathbf{Q}}(\mathbf{k}_X,\tau=\beta/2)=\frac{1}{2}\int_{-\infty}^{\infty} d\omega \frac{A(\mathbf{k}_{\mathrm{F}},\omega)}{\cosh(\beta\omega/2)}. \tag{5.1}$$

Similarly, a measure for the temperature dependence of the density of states at the Fermi energy $N(0)$ is obtained from the local Green's function (2.11), $z^*_{loc}(T)=-\Sigma_\sigma G_{\sigma\sigma\mathbf{Q}}(\tau=\beta/2)$. In the low-temperature limit, $N(0)$ can be obtained from the relation $N(0)\simeq\beta z^*_{loc}(T)/\pi$,[69] which gives

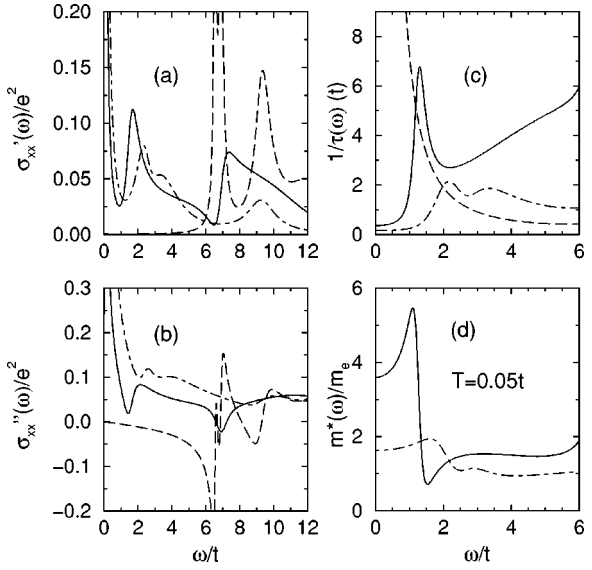

FIG. 16. Optical properties as functions of energy ω/t for the Hubbard model with extended hopping parameters of $La_{2-x}Sr_xCuO_4$ (Table I) at low temperature $T=0.05t$ for $\delta=0$ (dashed lines), $\delta=0.125$ (full lines), and $\delta=0.25$ (dash-dotted lines): (a) real part of the optical conductivity $\sigma'(\omega)$; (b) imaginary part of the optical conductivity $\sigma''(\omega)$; (c) scattering rate $1/\tau(\omega)$; (d) effective mass $m^*(\omega)/m_e$.

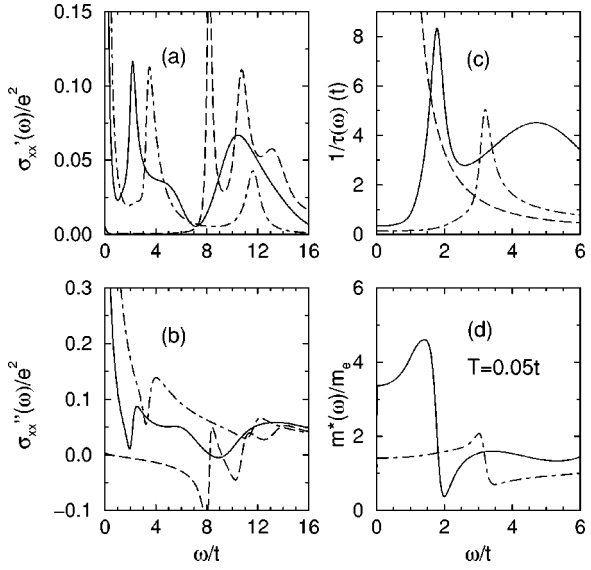

FIG. 17. Optical properties as functions of energy ω/t for the Hubbard model with extended hopping parameters of $YBa_2Cu_3O_{6+x}$ (Table I) at low temperature $T=0.05t$ for $\delta=0$ (dashed lines), $\delta=0.10$ (full lines), and $\delta=0.25$ (dash-dotted lines): the meaning of different panels is the same as in Fig. 13.

$\simeq 0.20$ ($\simeq 0.26$) for $\delta=0.125$ ($\delta=0.25$), respectively. However, one finds that the one-particle density of states at the Fermi energy does not evolve smoothly to low-temperature values, but instead states are depleted from the region $\omega\simeq\mu$ as T is reduced below $T^*\simeq 0.26t$ ($0.43t$) for $\delta=0.125$ ($\delta=0.25$), respectively. In particular, we observed a faster loss of the QP weight with momentum $\mathbf{k}_X=(\pi,0)$ for $\delta=0.125$ (Fig. 15). This shows that the opening of the pseudogap in the one-particle excitation spectrum at $(\pi,0)$ coincides with the suppression of the effective scattering rate $1/\tau(\omega,T)$.

Experimentally, the resistivity changes from a linear to a nearly linear T dependence at T^* of the order of 500 K. Although our calculations do not allow us to interpret the linear part of $\rho_{xx}(T)$ at high temperature $T>T^*$ as only the electronic degrees of freedom are included, we note that the enhanced slope of $\rho_{xx}(T)$ at low temperature $T\sim 100$ K and the negative temperature coefficient agree qualitatively with the experimental results for $YBa_2Cu_3O_{7-x}$ in the underdoped regime.[70] Our calculations confirm the conjecture of Shraiman and Siggia of a nearly linear T dependence of the resistivity for a system with SS magnetic order.[59] These features can be seen as generic fingerprints of incommensurate magnetic correlations.

B. Implications of extended hopping

Similar changes in the optical excitation spectra as a function of hole doping were also found using effective single-band models with parameters representative for $La_{2-x}Sr_xCuO_4$ (Fig. 16) and $YBa_2Cu_3O_{6+x}$ (Fig. 17), respectively. Due to somewhat larger values of the effective U, the gap in the optical spectra increases to $\sim 6.5t$ and $\sim 7.1t$ in these two compounds. One finds again that the Drude weight and the midgap state appear in the conductivity of doped systems. For the parameters of $La_{2-x}Sr_xCuO_4$ ($YBa_2Cu_3O_{6+x}$), the region of suppressed scattering extends up to $\simeq 1.3t$ ($\simeq 1.8t$) at $\delta=0.125$. This regime of low ω gives an enhanced effective mass $\sim 4m_e$ for both sets of model parameters. At larger doping $\delta=0.25$ the coherence of the charge carriers is enhanced by t' and t'' hopping, and one finds a significantly reduced effective scattering between charged carriers, extending with roughly no structure over a rather broad energy range. Simultaneously, the effective mass $\sim 1.5m_e$ is only little enhanced at low energies.

The overall shape of $\sigma'(\omega)$ (Fig. 16) shows a qualitatively similar behavior to the optical conductivity of $La_{2-x}Sr_xCuO_4$ reported by Uchida *et al.*[46] At low doping the midgap band centered at $\omega\simeq 1.7t$ (corresponding to 0.53 eV for $J=125$ meV and the present parameters with $J=0.4t$) is clearly distinguishable from the Drude contribution. It moves to higher energy $\omega\simeq 2.2t$ (0.7 eV) at $\delta=0.25$. It is quite remarkable that our DMFT calculations qualitatively reproduce the structures observed in the frequency dependent effective scattering rate $1/\tau(\omega)$ and in the effective mass $m^*(\omega)/m_e$ of $La_{2-x}Sr_xCuO_4$.[46] In particular, the strong doping dependence of $1/\tau(\omega)$ and $m^*(\omega)/m_e$ show the same trends, namely, a pronounced reduction of scattering and effective carrier mass for the heavily doped systems, and further justifies the importance of extended hopping parameters in the cuprates. This behavior originates from an increase of QP weight in the single-particle excitation spectrum induced by doping.

Puchkov *et al.*[71] reported extensive studies of the infrared properties of $YBa_2Cu_3O_{6+x}$, $Bi_2Sr_2CaCu_2O_{8+x}$, and other high-T_c compounds. They found that the far-infrared effective scattering rate $1/\tau(\omega)$ and the effective mass $m^*(\omega)/m_e$ differ significantly between underdoped and optimally doped samples above T_c. The optimally doped samples show a

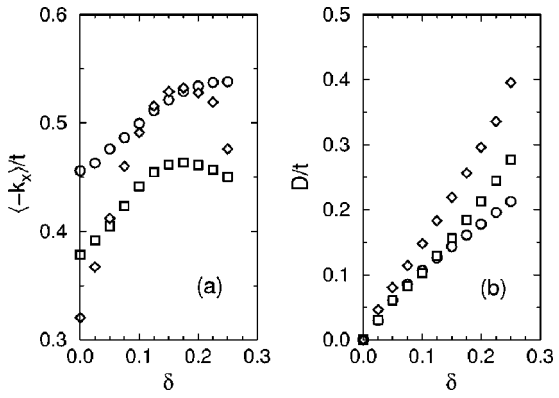

FIG. 18. Kinetic energy along the x direction $\langle -k_x \rangle / t$ and the Drude weight D/t as functions of the hole doping δ for representative values of parameters given in Table I: Hubbard model (circles), $La_{2-x}Sr_xCuO_4$ (squares), and $YBa_2Cu_3O_{6+x}$ (diamonds).

structureless and lower effective scattering rate $1/\tau(\omega)$, and a nearly constant and unrenormalized mass $m^*(\omega)$. Conversely, in underdoped samples the scattering between the charged carriers below ≈ 0.12 eV is strongly suppressed, and $m^*(\omega)/m_e$ is enhanced in the low-energy region. These observations are in remarkably good agreement with our findings, and support our conclusion that the observed doping dependence of $1/\tau(\omega)$ and $m^*(\omega)/m_e$ originate from an increased coherence of the one-particle excitation spectra reported in Sec. IV B, and experimentally observed in ARPES spectra of $Bi_2Sr_2CaCu_2O_{8+x}$ by Kim *et al.*[41] The suppression of $1/\tau(\omega)$ below $\omega \simeq 0.12$ eV originates from the opening of a pseudogap in the one-particle excitation spectrum. Using $J = 125$ meV and the value of $J = t/3$, adequate for $YBa_2Cu_3O_{6+x}$, we find the energy threshold below which QP scattering is strongly suppressed in the weakly doped system at $\simeq 0.68$ eV. Unfortunately, this is about a factor of 5 larger than the experimental value for underdoped $YBa_2Cu_3O_{6+x}$ being $\sim J$. Similar discrepancies in the energy of the QP state with momentum $(\pi,0)$ were reported in Sec. IV B.

C. Drude weight and spectral weight transfer

Finally, we compare the Drude weight D [Eq. (3.26)] and the kinetic energy density associated with x-oriented links $\langle -k_x \rangle$ [Eq. (3.16)] for the three model parameter sets in Fig. 18. DMFT gives $\langle -k_x \rangle = 0.46t$ for the Hubbard model at half-filling ($\delta = 0$) with $U = 8t$, which is smaller by a factor ~ 1.81 than the HF result, and is in excellent agreement with the value of $\langle -k_x \rangle = 0.49t$ obtained in QMC calculations.[56] We also found an overall satisfactory agreement of $\langle -k_x \rangle$ as a function of doping with ED data of Dagotto *et al.*[52] The kinetic energy $\langle -k_x \rangle$ increases with doping not only because the actual carrier density changes, but also as a consequence of changing wave vector in the SS state $\mathbf{Q} = [\pi(1 \pm 2\eta), \pi(1 \pm 2\eta)]$ with a gradually increasing pitch η allowing for coherent electronic transport through the system. In agreement with QMC data,[63] we observe that increased extended hopping amplitudes accelerate the SS formation and result in a stronger increase of $\langle -k_x \rangle$ with δ for $YBa_2Cu_3O_{6+x}$ than for $La_{2-x}Sr_xCuO_4$ model parameters. The x-directed kinetic energy shows a linear doping dependence in the regime of low hole doping, and $\langle -k_x \rangle$ changes by a factor of ~ 1.66 (1.22) with respect to half-filling in the case of the $YBa_2Cu_3O_{6+x}$ ($La_{2-x}Sr_xCuO_4$) model parameters; one finds a faster increase of the total spectral weight in the case of stronger hopping to second and third neighbors, as realized in $YBa_2Cu_3O_{6+x}$.

The calculated total optical spectral weights are $\propto \langle -k_x \rangle$, following the optical sum rule (3.22), and we made a quantitative comparison with the experimental data. The doping dependence of the total integrated spectral weight below the charge-transfer band edge at 1.5 eV, reported by Cooper *et al.*[72] for $La_{2-x}Sr_xCuO_4$, is strikingly similar to the numerical data of Fig. 18. The model reproduces a rapid increase of spectral weight up to $\sim 10\%$ Sr doping, and a rather doping-independent spectral weight in the range of $0.1 \leqslant x \leqslant 0.2$. The increase of $\propto \langle -k_x \rangle$ with increasing doping is faster for the parameters of $YBa_2Cu_3O_{6+x}$, with the integrated spectral weight increased by ~ 1.7 at $\delta = 0.18$ with respect to its value at $\delta = 0$. This value compares again very well, taking the simplicity of the effective single-band Hubbard model, with a factor of ~ 1.8 found by Orenstein *et al.*[73] in the compound with highest T_c.

At $\delta = 0$ we find a vanishing Drude weight for all three sets of model parameters, and the system is an insulator. This is of course an expected result at half-filling, but in the present context it serves as a test of the internal consistency of theory, like the kinetic-energy term $\langle -k_x \rangle \neq 0$ in Eq. (3.26), and has to be compensated for by the current-current correlation function $\Lambda_{xx}(\mathbf{q} = 0, 2\pi i T)$ in the limit of low temperature. At small hole doping we observed an almost perfect linear increase of the Drude weight with δ for all three sets of model parameters, which is an indication of strong electron correlations near the Mott insulator at half-filling.[64,74] Such a behavior is compatible with a picture of a dilute hole gas in a background with SS LRO which contributes to the optical response. However, the crossover to a metal due to increasing doping has been analyzed recently using scaling theory,[75] and ED technique combined with scaling theory,[76] which give $D \propto \delta^2$ for a small doping concentration δ in a 2D t-J model. This last result is in sharp contrast to the present picture of a dilute hole gas in an AF or SS background, and might indicate that other correlations are realized in the spin background when the system is doped, namely, that the dilute hole gas is unstable toward microscopic phase separation, such as realized in polaronic solutions or stripe phases.

The present results demonstrate a substantial transfer of spectral weight to low energy in the doped systems. We already pointed out earlier[24] that the spectral weight transferred into the LHB in the one-particle spectra agrees with the predictions of perturbation theory in the strongly correlated regime.[74] In the optical spectra for the Hubbard model at $U/t = 8$, one finds that the weight transferred into the region below the Mott-Hubbard gap is increased by a factor ~ 1.3 with respect to $\delta = 0.125$ when the system is doped to $\delta = 0.25$. This change is significant as the total weight obtained from Eq. (3.22) via $\langle -k_x \rangle$ remained roughly constant [see Fig. 18(a)], indicating a spectral weight transfer from the high- to low-energy region in the single-particle excitation spectrum.[74] In particular, the weight transfer is in favor of the Drude weight [Fig. 18(b)], which increased in the

same doping range by a factor ~ 2.15 although the hole density increased only by a factor 2. These changes in the coherent optical weight are consistent with the observation made in Sec. IV B that the single-particle excitation spectra become *more coherent* as the hole density increases.

VI. SUMMARY AND CONCLUSIONS

We reported a generalization of the DMFT to magnetically ordered states, and showed that this method allows for a very transparent study of spectral properties of the Hubbard model at and close to half-filling. The crucial step is the derived formula for the self-energy using the Berk-Schrieffer[38] spin-fluctuation exchange interaction with an effective potential due to particle-particle scattering.[34] We have demonstrated that this treatment of many-body effects reproduces the leading dependence on doping and temperature, and gives a very favorable comparison with the available numerical data obtained in the QMC and ED calculations for a 2D Hubbard model. Although the **k** dependence of the self-energy was not included, the spectral functions for a single hole in a Mott-Hubbard insulator agrees well with the known structure for the t-J model,[5] and gives a PES spectrum consisting of a *coherent* QP peak with a dispersion $\sim 2J$, and an *incoherent* part of width $\sim 7t$ at lower energies. We have verified that the QP weight agrees well with the ED data in the range of $J/t < 0.7$,[55] and supports the string picture.[77] Furthermore, the calculation reveals a nontrivial relation between the electron occupation factors $\langle n_{\mathbf{k}} \rangle$ and the QP weights $a_{\mathbf{k}}$, and shows that the maximum of $a_{\mathbf{k}}$ is shifted away from the $(\pi/2, \pi/2)$ point, in agreement with the ED results of Eskes and Eder.[57]

Our study has shown that doping of a Mott-Hubbard insulator leads to an incommensurate magnetic order at low temperatures, which depends on the actual values of the hopping parameters and the Coulomb interaction U. This kind of magnetic order induces a *pseudogap in the one-particle spectra*, which is one of the generic features of the doped Mott-Hubbard insulators. The dependence of the pseudogap on the incommensurate magnetic order explains why it could not be observed in ED data on small clusters at finite temperature,[66] or in the infinite-dimensional Hubbard model in the paramagnetic state.[78] This energy scale, due to a *pseudogap of magnetic origin*, demonstrates a combination of physics arising from the Slater picture and the Mott-Hubbard description of strongly correlated electron systems.

The coherent QP states survive in the doped systems, in agreement with QMC and ED results. However, the numerical studies suggest that a strong **k** dependence of the self-energy might be necessary to describe the spectra, as the QP dispersions change. This failure of the rigid QP band picture here has quite a different explanation: *the changes of the QP dispersion follow from the incommensurate magnetic order* which develops with doping, and the leading effects in the hole dynamics are still *captured by a local self-energy*.

The one-particle and optical spectra are interrelated, and the opening of a pseudogap at low temperatures leads to a midgap state next to the Drude peak in the optical conductivity, both with growing intensity under increasing doping. Such features, observed in SS states at low temperatures, as the suppressed scattering rate and the large effective mass in the underdoped regime, and almost no enhancement of the effective mass in a broad energy range in overdoped systems, are in remarkably good *qualitative* agreement with the experimental findings in the cuprates.[46,70] This is consistent with the reduced density of states $N(\mu)$ at the Fermi energy at low temperature. With increasing temperature the value of $N(\mu)$ increases, which could not be explained in paramagnetic calculations performed within the DMFT approach. It should be realized that such a strong temperature dependence of $N(\mu)$ should have important consequences for several measurable quantities in the normal phase, as for example the Knight shift.

Here we limited ourselves to the qualitative consequences of the extended hopping t' and t'' for the one-particle and optical spectra. First of all, the QP dispersion is strongly influenced by these parameters, and at half-filling reproduces the experimental width and dispersion of the QP band in $Sr_2CuO_2Cl_2$.[79] Second, the deviation of the characteristic **Q** vector from the AF vector (π, π) increases as a function of doping in SS states, and this process is accelerated by a finite value of second- (t') and third-neighbor (t'') hopping. This explains why systems with extended hopping are more metallic which is indicated by the low effective mass and larger Drude weight.

The dependence of the magnetic order on temperature has also rather drastic consequences for the measurable quantities. The onset of magnetic order below a characteristic temperature results in quite different one-particle and optical spectra at low temperatures from those obtained in a paramagnetic phase. The changes of the spiral **Q** vector with decreasing temperature allow one to introduce a crossover temperature T^*, below which the low-lying excitations are gradually modified along with the changes in local magnetic order. Such a modification gives a quasilinear resistivity, and verifies the conjecture of Shraiman and Siggia.[11]

In spite of very good agreement for the undoped systems, however, we identified several important features which do not agree with the experiments in the doped cuprates even on a qualitative level, that might indicate that a more accurate treatment of the many-body problem is necessary, or that more complex magnetic structures are stabilized in these compounds: (i) The value of the pseudogap in the one-particle spectra, and the accompanying energy scale for the suppressed scattering rate in the optical conductivity, are overestimated by a factor close to 5 with respect to the experimental observations. (ii) The SS(1,1) state obtained for the $La_{2-x}Sr_xCuO_4$ model parameters leads to a different splitting of the magnetic scattering peak in neutron experiments than the experimentally observed (1,0) and (0,1) splittings.[9] (iii) The incommensurate order deviates too fast from the AF state for the model parameters of $YBa_2Cu_3O_{6+x}$, which results in different spin-spin correlations than those observed in experiment, and a QP peak at the X point moving to too low energies.[40] (iv) The doping behavior of the pseudogap and of the related crossover temperature T^* is opposite to the one observed in the cuprates. In these materials the pseudogap and T^* decrease upon doping, whereas here the corresponding quantities increase from the $\delta = 0.125$ to the $\delta = 0.25$ case. With increasing doping charge fluctuations become more and more important, which gives rise to the suppression of magnetic order, and conse-

quently the pseudogap closes. However, such correlations are *underestimated* in the present treatment, and one instead finds a persisting pseudogap. (v) Finally, the spiral spin ordering in the (1,1) direction contrasts with experimental evidence from neutron scattering in the cuprates, suggesting that stripe ordering might play a prominent role in these systems at very low temperatures.[9,80] We have found a phase separation at low doping levels, and therefore the presently studied dilute hole gas in SS states is unstable toward magnetic polarons or stripe phases at doping levels lower than $\delta \simeq 0.1$. This motivates a further search for more complex magnetic ground states with incommensurate order, and more accurate methods to describe them in theory.

Summarizing, we presented a successful formulation of the DMFT for strongly correlated magnetic systems, which opens the possibility of further applications in transition-metal oxides. In contrast to earlier formulations based on the modified second-order formula for the self-energy,[19] the present self-energy, which describes dynamical effects in the propagation of a hole coupled to spin fluctuations, allows one to obtain stable magnetic solutions: AF ordering at half-filling and SS in doped systems. Although it is likely that better variational states, possibly with stripe ordering,[9,80,81] could be found, it is expected that the presented spectral and optical properties are generic for strongly correlated systems with an incommensurate order parameter. A better understanding of the cuprates, however, requires a further development of theory which should be able to capture the gradual changes of local magnetic correlations in doped Mott-Hubbard systems under increasing temperature.

ACKNOWLEDGMENTS

It is our pleasure to thank E. Arrigoni, P. Horsch, and D. Munzar for valuable discussions. A.M.O. acknowledges support by the Committee of Scientific Research (KBN) of Poland, Project No. 2 P03B 175 14.

[1] For a recent review, see M. Imada, A. Fujimori, and Y. Tokura, Rev. Mod. Phys. **70**, 1039 (1998).
[2] C.M. Varma, S. Schmitt-Rink, and E. Abrahams, Solid State Commun. **62**, 681 (1987); V. Emery, Phys. Rev. Lett. **58**, 2794 (1987).
[3] F.C. Zhang and T.M. Rice, Phys. Rev. B **37**, 3759 (1988).
[4] J.H. Jefferson, H. Eskes, and L. F. Feiner, Phys. Rev. B **45**, 7959 (1992); L.F. Feiner, J.H. Jefferson, and R. Raimondi, *ibid.* **53**, 8751 (1996).
[5] E. Dagotto, Rev. Mod. Phys. **66**, 763 (1994).
[6] J. Bała, A.M. Oleś, and J. Zaanen, Phys. Rev. B **52**, 4597 (1995); P.W. Leung, B.O. Wells, and R.J. Gooding, *ibid.* **56**, 6320 (1997); R. Eder, Y. Ohta, and G.A. Sawatzky, *ibid.* **55**, R3414 (1997); O.P. Sushkov, G.A. Sawatzky, R. Eder, and H. Eskes, *ibid.* **56**, 11 769 (1997); J. van den Brink and O.P. Shushkov, *ibid.* **57**, 3518 (1998).
[7] O.K. Andersen, A.I. Liechtenstein, O. Jepsen, and F. Paulsen, J. Phys. Chem. Solids **56**, 1573 (1995).
[8] L.F. Feiner, J.H. Jefferson, and R. Raimondi, Phys. Rev. Lett. **76**, 4939 (1996).
[9] J.M. Tranquada, J.D. Axe, N. Ichikawa, A.R. Moodenbaugh, N. Nakamura, and S. Uchida, Phys. Rev. Lett. **78**, 338 (1997); P. Dai, H.A. Mook, and F. Doğan, *ibid.* **80**, 1738 (1998); H.A. Mook, P. Dai, S. M. Heyden, G. Aepplie, T. G. Perring, and F. Doğan, Nature (London) **395**, 580 (1998).
[10] M.A. Kastner, R.J. Birgeneau, G. Shirane, and Y. Endoh, Rev. Mod. Phys. **70**, 897 (1998).
[11] B.I. Shraiman and E.D. Siggia, Phys. Rev. Lett. **62**, 1564 (1989); Phys. Rev. B **40**, 9162 (1989).
[12] C. Kübert and A. Muramatsu, Phys. Rev. B **47**, 787 (1993).
[13] J. Zaanen and O. Gunnarsson, Phys. Rev. B **40**, 7391 (1989); H.J. Schulz, Phys. Rev. Lett. **64**, 1445 (1990); M. Kato, K. Machida, H. Nakanishi, and M. Fujita, J. Phys. Soc. Jpn. **59**, 1047 (1990).
[14] E. Arrigoni and G.C. Strinati, Phys. Rev. B **44**, 7455 (1991).
[15] C.L. Kane, P.A. Lee, T.K. Ng, B. Chakraborty, and N. Read, Phys. Rev. B **41**, 2653 (1990).
[16] R. Frésard and P. Wölfle, J. Phys.: Condens. Matter **4**, 3625 (1992).
[17] J. Igarashi and P. Fulde, Phys. Rev. B **45**, 10 419 (1992).
[18] W. Metzner and D. Vollhardt, Phys. Rev. Lett. **62**, 324 (1989); E. Müller-Hartmann, Z. Phys. B **74**, 507 (1989).
[19] A. Georges, G. Kotliar, W. Krauth, and M.J. Rozenberg, Rev. Mod. Phys. **68**, 13 (1996).
[20] M. Jarrell, Phys. Rev. Lett. **69**, 168 (1992).
[21] D.E. Logan, M.P. Eastwood, and M.A. Tusch, Phys. Rev. Lett. **76**, 4785 (1996).
[22] H. Kajueter and G. Kotliar, Phys. Rev. Lett. **77**, 131 (1996).
[23] M. Potthoff, T. Wegner, and W. Nolting, Phys. Rev. B **55**, 16 132 (1997).
[24] M. Fleck, A.I. Lichtenstein, A.M. Oleś, L. Hedin, and V.I. Anisimov, Phys. Rev. Lett. **80**, 2393 (1998).
[25] R. Strack and D. Vollhardt, Phys. Rev. B **46**, 13 852 (1992).
[26] T. Pruschke, T. Obermeier, J. Keller, and M. Jarrell, Physica B **223-224**, 611 (1996).
[27] A. Khurana, Phys. Rev. Lett. **64**, 1990 (1990).
[28] M. Jarrell, J.K. Freericks, and T. Pruschke, Phys. Rev. B **51**, 11 704 (1995).
[29] T. Pruschke, M. Jarrell, and J.K. Freericks, Adv. Phys. **44**, 187 (1995).
[30] D. Vollhardt, in *Correlated Electron Systems*, edited by by V. J. Emery (World Scientific, Singapore, 1993), Vol. 9, p. 57.
[31] G. Baym, Phys. Rev. **127**, 836 (1962).
[32] V. Janiš and D. Vollhardt, Int. J. Mod. Phys. B **6**, 731 (1992); A. Georges, G. Kotliar, and Q. Si, *ibid.* **6**, 705 (1992).
[33] N.E. Bickers, D.J. Scalapino, and S.R. White, Phys. Rev. Lett. **62**, 961 (1989).
[34] L. Chen, C. Bourbonnais, T. Li, and A.-M.S. Tremblay, Phys. Rev. Lett. **66**, 369 (1991).
[35] M. Fleck, A.M. Oleś, and L. Hedin, Phys. Rev. B **56**, 3159 (1997).
[36] N. Bulut, D.J. Scalapino, and S.R. White, Phys. Rev. B **47**, 2742 (1993).
[37] J. Altmann, W. Brenig, A.P. Kampf, and E. Müller-Hartmann, Phys. Rev. B **52**, 7395 (1995).
[38] N.F. Berk and J.R. Schrieffer, Phys. Rev. Lett. **17**, 433 (1966).
[39] Y.M. Vilk and A.M.S. Tremblay, J. Phys. I **7**, 1309 (1997).

[40] D.S. Marshall, D. S. Dessau, A. G. Loeser, C. H. Park, A. Y. Matsuura, J. N. Eckstein, J. Bozovic, P. Fournier, A. Kapitalnik, W. E. Spicer, and Z. X. Shen, Phys. Rev. Lett. **76**, 4841 (1996).
[41] C. Kim, P. J. White, Z. X. Shen, T. Tolkyama, K. Shibata, S. Mackawa, B. O. Wells, Y. J. Kim, R. J. Birgeneau, and M. A. Kastner, Phys. Rev. Lett. **80**, 4245 (1998).
[42] L. Hedin and S. Lundquist, *Solid State Physics* (Academic Press, New York, 1969), Vol. 23, p. 1.
[43] C.-O. Almbladh and L. Hedin L, in *Handbook on Synchrotron Radiation*, edited by E. E. Koch (North Holland, Amsterdam, 1983), Vol. 1, p. 607.
[44] B.S. Shastry and B. Sutherland, Phys. Rev. Lett. **65**, 243 (1990).
[45] D.J. Scalapino, S.R. White, and S.C. Zhang, Phys. Rev. B **47**, 7995 (1993).
[46] S. Uchida, T. Ido, H. Takagi, T. Arima, Y. Tokura, and S. Tajima, Phys. Rev. B **43**, 7942 (1991); T. Startseva, T. Timusk, A. V. Puchkov, D. N. Basov, H. A. Mook, M. Okuga, T. Kimura, and K. Kishio, Phys. Rev. B **59**, 7184 (1999).
[47] K.A. Chao, J. Spałek, and A.M. Oleś, J. Phys. C **10**, L271 (1977).
[48] M. Ulmke, V. Janiš, and D. Vollhardt, Phys. Rev. B **51**, 10 411 (1995).
[49] T. Kennedy, E.H. Lieb, and B.S. Shastry, Phys. Rev. Lett. **61**, 2582 (1988).
[50] A. Singh and Z. Tešanović, Phys. Rev. B **41**, 614 (1990); **41**, 11 457 (1990).
[51] J.E. Hirsch and S. Tang, Phys. Rev. Lett. **62**, 591 (1989).
[52] E. Dagotto, F. Ortolani, and D.J. Scalapino, Phys. Rev. B **46**, 3183 (1992).
[53] S. Sorella, E. Tosatti, S. Baroni, R. Car, and M. Parrinello, Int. J. Mod. Phys. B **1**, 993 (1988).
[54] L.N. Bulaevskii, E.L. Nagaev, and D.I. Khomskii, Zh. Éksp. Teor. Fiz. **54**, 1562 (1968) [Sov. Phys. JETP **27**, 836 (1968)].
[55] G. Martínez and P. Horsch, Phys. Rev. B **44**, 317 (1991).
[56] N. Bulut, D.J. Scalapino, and S.R. White, Phys. Rev. Lett. **73**, 748 (1994).
[57] H. Eskes and R. Eder, Phys. Rev. B **54**, R14 226 (1996).
[58] E. Dagotto, A. Moreo, R. Joynt, S. Bacci, and E. Gagliano, Phys. Rev. B **41**, 2585 (1990); E. Dagotto, R. Joynt, A. Moreo, S. Bacci, and E. Gagliano, *ibid.* **41**, 9049 (1990).
[59] B. Shraiman and E. Siggia, Phys. Rev. Lett. **60**, 740 (1988).
[60] V.J. Emery, S.A. Kivelson, and H.Q. Lin, Phys. Rev. Lett. **64**, 475 (1990).
[61] P.G.J. van Dongen, Phys. Rev. Lett. **74**, 182 (1995); Phys. Rev. B **54**, 1584 (1996).
[62] N. Bulut, D.J. Scalapino, and S.R. White, Phys. Rev. B **50**, 7215 (1994); R. Preuss, W. Hanke, C. Gröber, and H.G. Evertz, Phys. Rev. Lett. **79**, 1122 (1997).
[63] D. Duffy and A. Moreo, Phys. Rev. B **52**, 15 607 (1995).
[64] C. Castellani, G. Kotliar, R. Raimondi, M. Grilli, Z. Wang, and M. Rozenberg, Phys. Rev. Lett. **69**, 2009 (1992).
[65] B. Battlogg, H. Y. Hwang, H. Takagi, R. J. Cara, and H. L. Kwo, Physica C **235-240**, 130 (1994).
[66] J. Jaklič and P. Prelovšek, Phys. Rev. B **50**, 7129 (1994); R. Hlubina and T.M. Rice, *ibid.* **51**, 9253 (1995).
[67] T. Pruschke and M. Jarrell, Phys. Rev. B **49**, 1458 (1994); G. Uhrig and D. Vollhardt, *ibid.* **52**, 5617 (1995).
[68] W.F. Brinkman and T.M. Rice, Phys. Rev. B **2**, 1324 (1970).
[69] N. Trivedi and M. Randeria, Phys. Rev. Lett. **75**, 312 (1995).
[70] T. Ito, K. Takenaka, and S. Uchida, Phys. Rev. Lett. **70**, 3995 (1993).
[71] A.V. Puchkov, D.N. Basov, and T. Timusk, J. Phys.: Condens. Matter **8**, 10 049 (1996); A.V. Puchkov, P. Fournier, D. N. Basov, T. N. Tiarsk, A. Kapitulnik, and N. N. Kolesnikov, Phys. Rev. Lett. **77**, 3212 (1996); D.N. Basov, R. Liang, B. Dabrowski, D. A. Bonn, W. N. Hardy, and T. Tiurnsk, *ibid.* **77**, 4090 (1996).
[72] S.L. Cooper, G. A. Thomas, J. Orenstein, D. H. Raphine, A. J. Millis, S. W. Cheong, A. S. Cooper, and Z. Fisk, Phys. Rev. B **41**, 11 605 (1990).
[73] J. Orenstein, G. Kotliar, H. Kajueter, G. A. Thomas, D. H. Raphine, J. M. Honig, and B. Metcalf, Phys. Rev. B **42**, 6342 (1990).
[74] H. Eskes and A.M. Oleś, Phys. Rev. Lett. **73**, 1279 (1994); H. Eskes, A.M. Oleś, M. Meinders, and W. Stephan, Phys. Rev. B **50**, 17 980 (1994).
[75] M. Imada, J. Phys. Soc. Jpn. **63**, 4294 (1994); **64**, 2954 (1995).
[76] H. Tsunetsugu and M. Imada, J. Phys. Soc. Jpn. **67**, 1864 (1998); M. Imada, F. Assad, H. Tsunetsugu, and Y. Motome, preprint, cond-mat/9808044.
[77] R. Eder and K.W. Becker, Phys. Rev. B **44**, 6982 (1991).
[78] T. Pruschke, D.L. Cox, and M. Jarrell, Phys. Rev. B **47**, 3553 (1993); M. Jarrell, J.K. Freericks, and T. Pruschke, Adv. Phys. **44**, 187 (1995); M.J. Rozenberg, G. Kotliar, H. Kajueter, G. A. Thomas, D. H. Raphine, J. M. Honig, and B. Metcalf, Phys. Rev. Lett. **75**, 105 (1995).
[79] B.O. Wells, Z. X. Shen, A. Matsuura, D. M. King, M. A. Kastner, M. Greven, and R. S. Birgeneau, Phys. Rev. Lett. **74**, 964 (1995).
[80] K. Yamada, C.H. Lee, Y. Endoh, G. Shirane, R.J. Birgeneau, and M.A. Kastner, Physica C **282-287**, 85 (1997).
[81] J. Zaanen, J. Phys. Chem. Solids **59**, 1769 (1998).